CHAPTER 1: INTRODUCTION

1.0 Background

Inductively coupled plasma atomic emission spectrometry (ICP-AES) and ICP-Mass Spectrometry (ICP-MS) have become extremely important tools for trace element analysis [1, 2, 3, 4, 5]. These techniques are generally superior in accuracy, precision, detection limits, dynamic range, and relative freedom from interference than other instrumental analytical methods. The use of automatic samplers, large computers, and appropriate software facilitates accurate and rapid analysis. One can analyze a solution for many elements in 1 minute using ICP-AES and hence large volumes of data can be generated very fast [1, 6].

However, although the analytical virtues offered by the techniques are not questionable, they both still suffer from interelement effects, albeit to a different degree. Special attention is drawn to the effects of elements with low ionization potentials (IP), known as easily ionizable elements (EIEs), on the excitation conditions and results of determinations. The Introduction of EIEs into the plasma may cause a change in the excitation temperature and electron number density, as well as a change in the spatial distribution of atomic and ionic species, and hence can have an impact on the excitation mechanism of the elements determined [1, 2, 3, 7, 8, 9]. Such EIEs turn up in a variety of samples where these techniques are employed, including geological samples, biological samples, and environmental samples [10]. One of the biggest dangers in ICP analysis today therefore, is the possibility of obtaining inaccurate results without any indication of a problem.

To try and mitigate for some of these complications, a number of useful remedial procedures have been adopted [11, 12, 13]. One such an approach is matrix-matching - adding pure substances to standard solutions in an attempt to

make their chemical, physical, and spectroscopic characteristics similar to that of the analyte sample. Unfortunately this approach is time-consuming and is only practical for samples whose chemical composition would have been previously characterised rigorously. Another approach is that of the standard addition method, whereby aliquots of known concentrations of each analyte element are added to the sample solution. A calibration plot can then be extrapolated to give the concentrations of the unknown, after dilution effects have been considered. However, such an approach is compromised in a truly multi-element analysis by the need to add many elements at the same time to the sample solution. These added elements may introduce interference themselves. A method that is fairly effective is to separate the analyte elements from the matrix. However the method is rather time consuming and also, is not entirely satisfactory since some analyte elements may also be lost together with the matrix. Some workers have suggested varying experimental parameters such as carrier gas flow, radio-frequency power, and viewing height until minimum effects are observed. However such an approach is uncertain. Results from fundamental research are needed to improve analysis accuracy, develop practical diagnostics and intelligent instruments, and reduce operator skill requirements [14, 15].

Over the years, improvements in sensitivity, precision and lowered interferences have been achieved as far as the empirical optimization of analytical performance. Noticeable improvements in these areas cannot be advanced significantly without a deeper fundamental understanding of the underlying processes involved in atom formation, excitation and ionization. Several workers [16-28] suggest that a more attractive approach to the problem of interferences from easily ionised elements has been to try and understand the fundamental

properties of the ICP, to understand what the relationship of the interferences is to plasma and sample characteristics, and through a rational plan, to eliminate them. Such an approach would however require an appreciation of the processes that occur in the plasma. However, although ICP has been around for about thirty years, mechanisms of analyte excitation and ionization are still not fully understood [29, 30]. Such mechanistic understanding is important to explain interference from the (EIEs). The result is that those matrix interferences that do exist are not easily explained [31].

1.1 Plasma Diagnostics

1.1.1 Formation of Inductively Coupled Plasma

The ICP is produced by passing initially ionized argon gas through a quartz torch located inside a Cu coil connected to a radio frequency (RF) generator [32-38]. The RF generator provides up to 3 kW forward power (in most commercial units) at a frequency of 27.1 MHz. The high-frequency currents flowing in the Cu coil generate oscillating magnetic fields whose lines of force are axially oriented inside the quartz tube and follow elliptical closed paths outside the coil. Electrons and ions pass through the oscillating electromagnetic field flowing at high acceleration rates in closed annular paths inside the quartz tube space. The induced magnetic fields' direction and strength vary with time resulting in electron acceleration on each half cycle [39, 40]. Collisions between accelerated electrons and ions, and ensuing unionised Ar gas cause further ionization. The collisions cause ohmic heating and, when measured spectroscopically, give thermal temperatures ranging from 6 000 to 10 000 K [39, 40]

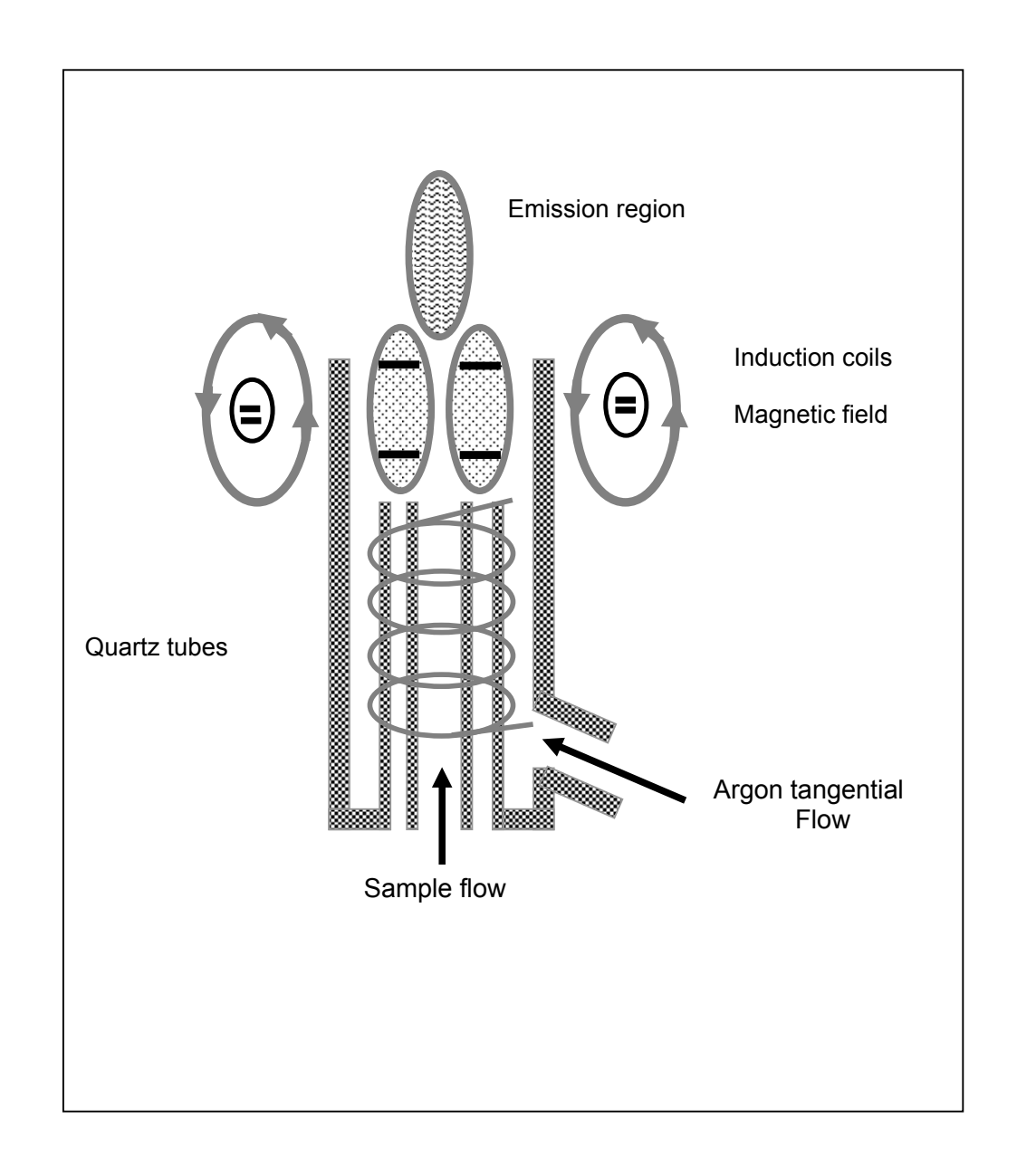


Fig. 1. Schematic diagram of an ICP Torch.

The quartz torch has three concentric channels. The outer channel conducts Ar gas at about 15 L min⁻¹ to 17 L min⁻¹ to the plasma to sustain the plasma, and to isolate the quartz tube from high temperatures [39, 40]. The innermost channel is for introduction of sample into the plasma. The middle channel conducts the auxiliary argon gas at about 1 L min⁻¹ and is used when starting the plasma only or for organic samples. The ICP has an annular, or donut, shape when viewed from above (Fig 1). Power dissipation is confined to the outer zones meaning that the axial zone in the centre has a relatively lower temperature than the donut body. The cool centre forms a weak spot so that it is relatively easy to inject a gas stream (containing sample aerosol) through the centre without disturbing plasma stability. The sample is therefore heated from the outside by the surrounding plasma, and it experiences high temperatures for relatively long periods of time, hence giving high residence times [38, 39, 40].

1.1.2 Plasma zones

There is some confusion when dealing with the spatially resolved interelemental matrix effects regarding the criterion to indicate the exact plasma region that is being monitored [38, 39]. The plasma central channel can be divided into three different zones; a pre-heating zone (PHZ); the so-called *initial radiation zone* (IRZ), in which the atomic emission begins to be observed; and the *normal* analytical zone, (NAZ) which corresponds to the zone at which emission is produced mainly from ions (about 14 to 19 mm to the tip of the IRZ). In the NAZ few inter-element effects exist [38, 39].

The IRZ extends upward to one or two mm above the load coil, taking on the appearance of an amber bullet during the nebulization of many sample types containing calcium. The IRZ is the plasma region where elemental matrix effect is strongest and must be avoided in analytical measurements [41, 42]. In many cases, the variation of the matrix effect with rf power and gas flow rate (Q_g) can be explained by a shift of the IRZ, because an increase in the Q_g and a decrease in rf power move the IRZ up.

Easily ionized elements lead to shifts in the spatial plasma non-homogeneous distribution of the analyte emitting species [43, 44]. The axial and radial observation position in the plasma influence the extent of the EIEs. The spatial effects can explain some contradictory results found in the literature concerning the role of the EIEs.

1.1.3 Fundamental Parameters and Plasma characteristics.

1.1.3.1 Debye length

Although a plasma contains both charged and neutral particles (electrons, ions, atoms and molecules), it remains quasi neutral because around each charged particle are distributed those of opposite charge. As a result of this distribution, the Coulomb force of each charged particle is shielded on a scale called the Debye length λ_D given by [45]:

$$\lambda_D = \left[kT_e / 4\pi n_e e^2 \right]^{1/2} \tag{1}$$

where k is the Boltzmann constant, T_e the electron temperature, n_e the electron number density and e the charge of an electron. The shielding length grows with electron energy (kT_e) but decreases at high electron number density (n_e) . The

Debye length is significant in the definition of a plasma. A criterion for an ionized gas to be a plasma is that the gas should be dense enough that λ_D is much smaller than the dimensions of the gas. For an ICP, the values of λ_D are of the order of 10^{-5} – 10^{-6} cm.

1.1.3.2 Local thermodynamic equilibrium

Local thermodynamic equilibrium (LTE) is a situation where all of the equilibrating processes in the system are due to collisional processes and all radiative processes contribute to such a small degree to the total energy of the system that they can be neglected [46, 47]. In an LTE system, the relative populations of the energy levels within any ionization stage can be calculated by the Boltzmann equation [39, 48]:

$$\frac{n_2}{n_1} = \frac{g_2}{g_1} \exp{-\left(\frac{E_2 - E_1}{kT}\right)}$$
 (2)

and the relative ion levels populations of two adjacent ionization stages can be calculated using the Saha equation [39, 48]:

$$\frac{n_3}{n_1} = \frac{6.037x10^{21}}{n_e} \cdot \frac{g_3}{g_1} T_e^{3/2} \cdot \exp\left\{\frac{-(E_3 - E_1)}{kT}\right\}$$
(3)

where levels 1 and 2 are levels from some ionization stage (densities in cm^{-3}), and 3 is a level in some higher adjacent stage, g is the statistical weight, T_e is the electron temperature in eV, E is the energy of a level (vs the ground atomic state value of zero) in eV, and n_e is the electron density.

The Boltzmann distribution is maintained from the principle of detailed balance of the collisional excitation rates and decay (superelastic) rates for atom-

electron collisions in the plasma. The equation depends on a Maxwellian distribution of electron velocities. The Saha equation likewise is maintained from a detailed balance argument, but between electron-atom collisional ionization rates and three-body re-combination rates [48].

1.1.3.3 Departures from thermal equilibrium

Only excited atoms or ions produce emission. The mechanisms for excitation and ionization are of interest because equilibrium-based expressions do not correctly predict experimentally measured emission intensities. If the ICP were in local thermodynamic equilibrium, relative emission intensities and the extent of ionization would be easy to predict. This would have implications on semi quantitative analysis using ICP-OES [49].

However, it is now generally accepted that the inductively coupled plasma operated in argon is not in local thermodynamic equilibrium, at least in the region used for analytical observations between 5 and 30 mm above the rf — coil. The results of various studies [49-51] can be summarised by the following statements; (i). the observed concentrations of electrons and hence of argon ions ranging from 10^{14} cm⁻³ to 10 cm⁻³, while explaining the absence of ionization interference in the argon ICP, cannot be reconciled with spectroscopically measured excitation temperatures using two-line or many-line technique; (ii) the values found for such excitation temperatures increase with upper energy of the transitions considered or, in other words, the relative overpopulation of an energy level increases with its excitation energy; and (iii) the intensity ratio of an ion line and an atom line of the same element is again significantly higher than expected from LTE expressions using excitation temperatures.

These observations may be expressed succinctly as [52]:

$$T_{Arion} > T_e > T_{ion} > T_{exc} > T_g$$

where $T_{Ar\ ion}$ is the argon ionization temperature, T_e is the electron temperature, T_{ion} is the analyte ionization temperature, T_{exc} is the analyte excitation temperature, and T_g is the gas or heavy particle temperature.

1.1.3.4 Temperature and electron number density

The emission intensity which is observed when elements are analysed spectrochemically using Inductively Coupled Plasma (ICP) is a function of both temperature and electron number density since these parameters determine the relative populations of analyte atom and ion species, and the excited state populations of these species [53-60]. During the plasma initiation process, radio frequency power is initially coupled to the ICP by the acceleration of electrons in the field induced by the load coil [39, 61]. Because of the difference in mass, ions pick up *rf* energy less efficiently than electrons. Therefore electrons initially gain *rf* energy in the induction zone and rapidly transfer it to ions and, indirectly, to neutral atoms. However since the collisional cross-section between electrons and ions is much larger than between electrons and atoms, ions gain energy from electrons much faster than atoms [62]. As a result, electrons will be described by a temperature greater than ion temperature which in turn will be greater than neutral atom temperature. That is, electron temperatures depart substantially from the heavy particle (or gas – kinetic) temperature.

From the foregoing discussion, it is not surprising therefore that various authors have measured electron number density and temperature in the ICP [63-81]. The values obtained vary considerably, but have in general been between 10¹³

- 10¹⁶ electrons per cubic centimetre (cm⁻³). The variation is attributable to the spatial inhomogeneity of the plasma. Although an electron number density, n_e can be determined without any assumptions about local thermal equilibrium (LTE), a single temperature cannot be determined explicitly because LTE does not exist in the ICP. Several temperatures have been defined for the ICP, including electron temperature (T_e), ionisation temperature (T_{ion}), gas temperature (T_g) and excitation temperature (T_{ex}) [79, 82]. It would be inappropriate to estimate electron temperature by assuming its equality with the excitation temperature of a thermometric species or with the ionisation temperature of the plasma support gas. Electron temperatures should be measured explicitly.

Methods that have been used to measure electron density in ICP include the Saha-Eggert ionisation equilibrium method, the line merging at series limit, and stark broadening of spectral lines [39, 83-85]. The Saha-Eggert method is based on the measurement of the relative intensities of neutral atom and single ionised emission lines of the same species and substitution of this ratio into a Saha equation along with an appropriate temperature. The limitation of this approach is on which of the temperatures; electron temperature, gas kinetic temperature and excitation temperature the determination should be based.

The line merging technique is based on the fact that as the principal quantum number increases, the wings of the Stark-broadened lines start to overlap each other until finally, before reaching the series limit, the lines merge completely, giving a continuum. The principal quantum number at which this merging occurs is found to depend on n_e. However the limitation of this technique is that defining the "Last discernible line" is not precise [39].

Stark broadening arises from the perturbation of the energy levels of emitting (or absorbing) species by an electric field caused by the motion of and concentration of charged particles. Stark broadening of spectral lines emitted by argon or hydrogen are mainly used. For example, the spatially resolved radial electron density at a given vertical height above the load coil is given by [39]:

$$n_e(r) = 7.9658 \times 10^{12} \left(\Delta \lambda_{1/2}(r) / \alpha_{1/2} \right)^{3/2}$$
 (4)

where $\Delta \lambda_{1/2}$ (r) = the radial full half width of H_{β} line,

 $\Delta \lambda_{1/2}$ = reduced half width parameter.

There are several limitations in the application of the Stark broadening method. The method requires the assumption that electron temperature is the same as excitation or ion temperature, and demands knowledge of accurate stark parameters. In addition, the lateral emission signals obtained in these measurements must be Abel–inverted to generate radial maps. Also, the experimental Stark–broadened line profile must be de-convoluted to correct for instrumental and Doppler broadening and measurement errors can be associated with all of these operations. Another limitation is that the experimental procedure is laborious since measurement of the intensity distribution over the line profile and determination of the background level of the adjacent continuum is necessary [39].

Techniques involving the use of sophisticated equipment has been applied by several workers to characterise the fundamental properties of the plasma [86-90] have described a suite of techniques that can enable mapping of the plasma features on a spatially resolved basis. The methods involve a combination of

Thomson scattering, Rayleigh scattering, computed emission tomography, and laser-induced saturated fluorescence.

Thomson scattering is the scattering of electromagnetic radiation from free electrons [55-60]. Because electrons are small and because of high temperature that exists in an ICP, the electrons move at extremely high velocities, on the 10⁶ m/s. This high velocity imparts to the scattered light a substantial Doppler shift, large enough that it can be measured with a conventional optical spectrometer. Because the electrons travel at random directions with respect to both the laser and the direction of observation, a distribution of Doppler Shifts is recorded an can be as broad as 5 nm. From this distribution of Doppler shifts can be obtained the electron energy distribution and, in the case of the ICP where a Maxwellian distribution exists, an electron temperature, T_e. In addition, the integrated Thomson-scattering spectrum indicates the number of electrons that are present in the viewing volume, so use of a calibrated spectrometer enables the electron number density to be determined at the same time [55-60].

Rayleigh scattering arises from the interaction of the incident laser beam and large particles, the greatest of which in an ICP are neutral argon atoms [57-60]. Because the atoms are large, their velocities are far lower than those of the electrons, so the Rayleigh-scattering peak lies at the same wavelength as the incident laser and therefore can be distinguished readily from the broader Thomson-scattering profile. The intensity of the Rayleigh-scattering is proportional to the number density of argon atoms in the viewing volume. In turn, this number density is inversely proportional to the gas-kinetic temperature, in accordance to Gas Law. A calibrated spectrometer would therefore enable determination of gas-kinetic temperatures on a spatially and temporary resolved basis at the same time

a Thomson-scattering spectrum is being recorded [68, 79, 85]. Monning *et al.* [59, 91] have used computed emission tomography employing a conventional photographic camera (with a monochromator standing in place of the aperture in the conventional system) to unravel a full three-dimensional structure of the plasma. Collection of such images over a large number of angles spanning a range of 180 degrees has permitted the three-dimensional structure of the plasma discharge to be displayed, regardless of the lack of plasma symmetry.

Laser-induced saturated fluorescence has been employed to collect time-resolved spatial maps of ground-state analyte atoms and ions and also of argon excited states [92-94]. Hieftje *et al.* [95] have applied the same optical arrangements as employed in Thomson-scattering, with the frequency-doubled (532 nm) Nd-YAG laser used in Thomson-scattering being replaced by the beam from a tunable dye laser pumped by the same Nd-YAG unit.

Using the techniques described in the preceding paragraphs, Hieftje *et al* have probed the mechanisms of analyte atoms and ions excitation in the ICP. They have concluded that collisional processes involving electrons are likely to play a major role in the excitation processes [95].

Van der Sande *et al.* [45] reported an approach to determine the internal plasma parameters (electron temperature, gas kinetic temperature, and electron number densities) using input parameters (carrier gas flow rate, r.f power, initial gas temperature and gas density). The equations used are also based on Thomson-scattering and relate the experimental scattering intensity I_T to the electron density by [45]:

$$I_T \alpha \left(\frac{n_e}{1 + \alpha^2} \right) \tag{5}$$

where the scattering parameter α represents the degree of coherence of scattered radiation and is given by [45]:

$$\alpha = \frac{1}{\kappa \lambda} = \frac{\lambda_i}{4\pi \sin(\theta/2)\lambda_p} \tag{6}$$

Where $\kappa = 4 \pi \sin (\theta/2) / \lambda_i$ is the length of the scattering vector K, θ the angle between incident and scattered radiation, λ_i the wavelength of incident radiation and $\lambda_D = (\varepsilon_0 k_B T_e / e^2 n_e)^{1/2}$, the Debye shielding length, in which ε_0 is the electric constant, k_B the Boltzmann constant, and e^- the elementary charge.

The electron number density is then given by [45]:

$$n_e = n_{Ar} \left(\frac{I_T}{I_R} \right) \left(\frac{1 + \alpha^2}{147} \right) \tag{7}$$

where, I_R is the intensity produced by Rayleigh scattering on Argon of known density n_{Ar} , the factor (1 / 147) is the ratio of the cross – sections of Rayleigh scattering at a wavelength of λ_i = 532 nm.

Consideration of Doppler broadening and coherent effects enable determination of both T_e and α from the Thomson-scattering spectrum. The average heavy – particle temperature is given by [45, 96]:

$$\langle T_h \rangle \approx T_0 + \frac{p}{\varphi \rho c_p}$$
 (8)

where P is the dissipated power, $c_p \approx 520 \text{ j Kg}^{\text{-1}}\text{K}^{\text{-1}}$ the heat capacity of Argon, $\rho \approx 1.79 \text{ Kg m}^{\text{-3}}$ the mass density at room temperature, and φ the total argon flow at room temperature. T_0 is the temperature of the gas before entering the plasma.

For various ICP conditions, the electron temperature is given by [45]:

$$\frac{k_B T_e}{E_{12}^*} = \frac{1}{46.6 + 2\ln\Lambda_{ne} - 2\ln T_h} \tag{9}$$

where Λ_{ne} is the gradient length, E^*_{12} the excitation energy, k_B is the Boltzmann constant and T_h the heavy particle temperature.

Using these expressions, M.J. van der Sande *et al.* [45], demonstrated that the behaviour of the internal plasma parameters can be estimated on the basis of operational conditions of the plasma and advantages of this method include; (i) direct and simultaneous measurement of spatially resolved electron temperature or electron energy distribution and electron number density without the need for assuming thermal equilibrium or performing Abel inversion; and (ii) Temporal resolution, depending on laser pulse length; as a result, Q-switched laser can be used to study temporal behaviour of the plasma. However, it can be noted that the need to make estimations of power density ε , the gradient length Λ_{ne} and T_h places a limit to the applicability of the method as that may be a major source of deviations in the values obtained.

1.2 Effect of easily ionized elements on line emission intensity

Easily ionized elements are found among different elements which constitute the matrix in liquid samples. The EIEs have traditionally been those most studied in the field of elemental matrix effects in ICP-AES. This is due to several reasons, among them (i) historical tradition, since the effects of the these elements have been widely studied in flames [97-103]; (ii) the effect of EIEs in ICPs is less pronounced than in flames and other types of plasmas such as the dc plasmas [104] (iii) the effects produced by EIEs are more pronounced than those observed for non EIEs; (iv) there are many samples containing high concentration of these elements; and (v) In spite of the huge volume of work reported, there is still no agreement on the dominant mechanism [105-126]. However, it is not only the low IP elements that cause a matrix effect. Elements with a higher IP also have been shown to give rise to similar effects on the analytical signal.

The effect of EIEs on plasma spectrochemical techniques is rather complex and "studying the literature on these interferences in the ICP is a study of confusion" [31]. Blades and Horlick [31] initially attributed this confusion to the inconsistency of the data that had appeared in the literature concerning these matrix effects, because some workers had found enhancements, depressions or no effects at all on the analytical signal when EIEs were present. In addition, there is no satisfactory mechanistic account of how the interferences are produced. As noted by various authors, [31, 100-102], the sources of EIEs interferences are not fully characterized.

There have been therefore a number of publications on modeling of the effects of EIEs, in a field that has become to be known as plasma diagnostics [7-9, 13, 22, 31, 43, 44, 62, 97-102, 126-134]. Plasma diagnostics is concerned with

studying processes occurring within the plasma. Current plasma diagnostic methods can be classified into three approaches: (a) active methods, (b) passive methods and (c) rate models.

1.2.1 Active methods

Active methods involves mapping of plasma features on a spatially and temporally resolved basis [67-70]. Key parameters in this approach to plasma diagnostics are the electron number density (n_e), electron temperature (T_e), the gas kinetic temperature (T_g), and argon atom number density (n_{Ar}). The methods employed involve a combination of Thomson scattering, Rayleigh scattering, computed emission tomography and laser-induced saturated fluorescence [63-81]. Thomson scattering enables measurement of T_e and n_e . The intensity of the Rayleigh scattering is proportional to n_{Ar} , which in turn is inversely proportional to T_g . Computed emission tomography enables the display of the full three-dimensional structure of the plasma torch. Laser-induced saturated fluorescence employs the same arrangement as used for Thomson scattering, and yields time-resolved spatial maps of ground state analyte atoms and ions, as well as argon excited states.

Although considerable success has been achieved in the determination of the electron number density (n_e) , electron temperature (T_e) , the gas kinetic temperature (T_g) and the argon atom number density (n_{Ar}) , it has been found that values of T_e and n_e in the ICP depend upon plasma configuration and measurement procedure. In addition, it is now generally accepted that the ICP is not in LTE [14].

1.2.2 Passive methods

The passive approach involves monitoring the behaviour of the plasma itself. In an outstanding paper, Blades and Horlick [31] carried out a more systematic study, and plotted the variation of the relative intensity (i.e., the emission intensity in the presence of interferent with respect to that in the absence of interferent) for the effects of excess Li, Na, and K on the emission of Ca, Cd and Cr. They focused on (a) the vertical profiles of the interference effects, (b) radial profiles, (c) effect of varying the interferent, (d) effect of varying rf power, (e) nebulizer effects, and (f) ionization equilibria effects. They found that the relative emission intensity was maximum at 7 mm alc. The matrix effect disappeared for both lines at 17 mm alc, a "cross over" point being obtained. At plasma observation heights above this, the relative intensity dropped. According to these workers, the position of the cross over point did not change as a function of the sodium concentration. On the basis of these investigations, Blades and Horlick [31] concluded that (a) for both atom and ion lines, the addition of excess EIE's enhances the emission in the lower regions of the ICP discharge, but leads to depression of the emission signal in the upper regions of the discharge; (b) low in the discharge emission, enhancement appears to be the result of an increase in collisional excitation; and (c) higher in the discharge, depression of emission signal appears to result from ambipolar diffusion. The contribution of shifts in ionization equilibria was discounted on the grounds that the emission enhancement was not accompanied by a corresponding increase in ground state populations.

Wu and Hieftje [127] measured, under non-robust conditions (i.e., rf power 0.8 kW; Q_g , 1.2 lmin^{-1}), the Na emission signal in the presence of other easily ionized elements such as lithium, potassium, and caesium, finding that the signal

Increased in the presence of these elements for almost all heights investigated. The cross over point was located at around 14-15 mm alc, the Na emission signal about the same for all the solutions tested. In a different publication, Hieftje and coworkers [43, 44] carried out an exhaustive spatial study on the interferences of lithium on Cal and Call emission intensities. They plotted bidimensional Ca atomic and ionic emission maps by using a monochromatic imaging spectrometer and then applying the Abel inversion procedure to obtain the radial emission images. The results showed that for Cal emission, the matrix effects were more pronounced off-axis high in the plasma and both on-axis and off-axis low in the plasma. For Call the interferences existed on-axis from 5 to around 18 mm alc. The conclusions drawn concerning the lithium effect on Ca emission intensities were [43, 44]; (i) off axis regions never showed depression in atomic or ionic emission; (ii) on-axis positions never showed ionic emission enhancements; and (iii) the atomic emission was enhanced, depressed or unchanged in on-axis locations.

1.3 Models used in the passive methods

1.3.1 The radiation-trapping model

The radiation-trapping model proposed by Blades and Hieftje attempted to explain the overpopulation of high energy levels, notably of argon metastable levels [41]. Although spectral transitions between the metastable levels and the ground state are forbidden, there are other argon levels of high energy that do couple radiatively with the ground state. The authors argue correctly that closely spaced energy levels equilibrate rapidly through collisions. They then propose that a high population of radiative levels of argon atoms in the cool zones of the argon

ICP is maintained by absorption of far UV radiation (100 nm) emitted by hot outer plasma ring. The ensuing high population is rapidly transferred to the metastable levels. The argument, however, appears to be much too incomplete to be considered as a full-fledged excitation model. The authors do not attempt to estimate the concentration of metastable argon atoms that would result from this phenomenon. They do provide, however, an apparent lifetime of radiative levels of 10⁻³ s, which is five orders of magnitude more than the normal radiative lifetime of 10⁻⁸ s. The latter would apply to plasma in thermal equilibrium, where the principle of detailed balancing would apply. The contribution of radiation trapping would therefore lead to an argon metastable concentration of at most 10⁹ atoms cm⁻³, a value too low to explain the suprathermal ionization of analyte atoms. It is, therefore, unlikely that radiation trapping could explain a suprathermal concentration of argon metastables in the analytical observation zone of the argon ICP. Mills and Hieftje, in an oncoming publication [106] conceded that radiation trapping couldn't be responsible for sustaining the plasma well beyond the coil region. It was also noted that the model falls short to reconcile the high electron number density observed for the plasma $(10^{15} - 10^{16} \text{ cm}^{-3})$ with the high degree of analyte ionization [106].

1.3.2 The argon-metastable model

This model seeks to explain the observed high ion/atom intensity ratios in terms of a high population of metastable argon energy levels [41]. The term level for a noble gas element consists of singlet and triplet levels. In argon, the ground state is ${}^{1}S_{0}$ and the next four higher levels are a ${}^{3}P_{2,1,0}$ and a ${}^{1}P_{1}$, all clustered between 11.5 to 11.8 eV above the ground state [41]. Of these four levels, the ${}^{3}P_{1}$

and ${}^{1}P_{1}$ levels allow radiative transitions to the ground state, but the transition from ${}^{3}P_{2}$ and ${}^{3}P_{0}$ to the ground state would require spin flip and are not observed. As a result, their radiative lifetimes are extremely long and the levels are called metastable. The rest of the higher energy levels all couple radiatively to lower singlet or triplet levels. However, for the argon ICP at atmospheric pressure, the dominating processes are collisions with a rate of about 10^{9} s $^{-1}$, implying that all the four argon levels at 11.54 to 11.82 eV have similar actual lifetimes and hence are populated to the same degree. This is in agreement with Blades and Hieftje [41], who have suggested that there is really nothing mysterious about the metastable argon levels. A critical analysis by de Galan [114] also revealed that proposals of a special role of metastable argon atoms are speculative rather than convincing. The arguments presented by Boumans and de Boer are based on experimental evidence rather than theoretical explanation and lack a quantitative basis in terms of reaction rate constants.

1.3.3 The ambipolar diffusion model

Several workers have considered ambipolar diffusion to be important [87, 88, 89, 135]. Light charged particles (electrons) tend to diffuse in the plasma more efficiently than heavier ones (analyte, matrix). As a result of these movements, a charge separation between the electrons and the heavy – particle ions can be observed thus generating an electric field. The potential of this field tends to increase the diffusion rate from lower to higher electron density zones for heavy ions and to decrease this rate for the light particles. Neutral atoms are not affected by this process. The ambipolar diffusion model, proposed by Aeschbach, differs from the models discussed so far in that the latter makes explicit assumptions

about the temperature and electron concentration in the argon ICP whereas these quantities are calculated from incident rf-power transferred by the coil to the plasma where ambipolar diffusion is considered [31]. The author postulates a two-temperature model, where the kinetic temperature of atoms and ions is significantly lower than the temperature of the electrons. Electrons are generated in the hot plasma ring inside the coil region and migrate into cooler zones inside and above the plasma ring through axial convection and ambipolar diffusion. These processes are given by the equations:

$$\Gamma_a = D_a V^2 n_e$$
 (ambipolar diffusion) (10)

$$\Gamma_c = -\nu \nabla n_e$$
 (convection) (11)

where Γ is the number of electron - Ar ion pairs flowing into a unit volume at the location (x, y,z) per second, D_a is the ambipolar diffusion coefficient, and v is the gas velocity.

The model succeeded in the calculation of spatial distribution of electron concentration and the two temperatures in two actual argon ICPs taken from the literature when applied by the author. High electron concentrations were shown to persist up to 30 mm above the rf-coil in the centre of the plasma and this was explained in terms of the inefficient transfer of energy from "hot" electrons to "cool" atoms and seconds the slow recombination of argon ions and electrons. However as the author admits, the ambipolar diffusion model cannot explain the relative population of various energy levels of one species and the increase of the excitation temperature with excitation energy, a variation which would complicate his crude two-temperature model. In this sense, the proposal is not a complete

excitation model [31]. The model however shows that the high electron concentrations observed in the argon ICP can arise from simple mechanical processes starting from a thermal plasma region inside the rf-coil.

1.3.4 The reaction rate model

Finally, one approach that has attracted significant attention is the reaction rate model which can take a classical or simplified approach.

1.3.4.1 Classical rate model

The classical collisional-radiative rate model approach takes into account all possible electronic states of the analyte and matrix and the level populations are derived from the excitation and de-excitation reactions occurring in the plasma. A number of possible interactions may occur between particles. The following is a list of the most significant mechanisms that have been proposed for excitation in the ICP.

1.3.4.1 (a) Collisional excitation and de-excitation by electrons

Collisional excitation is the transition of a bound orbital electron in an atom (or ion) of analyte species M to a higher bound state by the absorption of kinetic energy by inelastic collision with a free electron [136]. When the transition is between levels p and q at energies E_p and E_q the process is represented by [95]:

$$M_q + e \rightarrow M_p + e$$
, where $E_p > E_q$ (12)

The corresponding inverse process of de-excitation is represented by [95]:

$$M_p + e \rightarrow M_q + e$$
, where $E_p > E_q$ (13)

1.3.4.1 (b) Radiative decay

De-excitation of species M_p (or M_p^+) can proceed via spontaneous radiative decay, with emission of a photon of energy $h\nu_{line}$ according to [95]:

$$M_p \to M_q + h v_{line}$$
 and (14)

$$M^{+}_{p} \to M^{+}_{q} + h \nu_{line}$$
 (15)

Spontaneous radiative decay is likely to be the primary depopulating process when there are large energy differences between bound levels and relatively low electron densities.

1.3.4.1 (c) Collisional ionization and three-body recombination

The presence of EIEs might also cause an enhancement in the collisional processes [31, 137]. An increase in the electron number density can also produce a rise in the number of collisions thus giving support to an enhancement of both atomic and ionic emission line intensities. A neutral atom or an ion of species M may become further ionized by impact of a colliding electron whose kinetic energy is greater than the binding energy of a particular orbital electron; i.e., the threshold energy for ionization. The process is represented by [95]:

$$M_n + e \to M^+ + 2e \tag{16}$$

The inverse of this process is three-body recombination, represented by [95]:

$$M^+ + 2e \rightarrow M_n + e \tag{17}$$

The excess energy released in this inelastic process is carried off by the second free electron.

1.3.4.1 (d) Radiative recombination

Recombination of a free electron with a positive ion of analyte species M⁺ may proceed by radiative recombination described by [95, 138, 139]:

$$M^{+} + e \rightarrow M_{n} + h v_{cont} \tag{18}$$

1.3.4.1 (e) Charge transfer

The transfer of charge between heavy particles may occur through several processes. In the ICP, charge transfer between argon and analyte atoms is represented by [140-146]:

$$Ar^{+} + M_{q} \rightarrow Ar + M^{+}_{p} \tag{19}$$

The result of the reaction is an excited state analyte ion. The energy difference (defect) between the argon ion and the resulting analyte ion should not be too large for there to be favourable cross sections.

1.3.4.1 (f) Penning ionization and excitation

The role of the argon metastable species, Ar_m , in ICP excitation has been investigated and speculated upon by several researchers [118, 119, 122, 147]. The process is represented by [118, 119]:

$$Ar_m + M \to Ar + M^+_p + e \tag{20}$$

The production of a ground state analyte ion or excited analyte ion depends on the energy involved. Excess energy is carried away by the electron. Thus, the high electron density observed in the plasma (higher than expected from the measured excitation temperatures and assuming LTE) might be related to an overpopulation of argon metastable atoms, which could be related act as an ionization buffer.

1.3.4.1 (g) Shifts in ionization equilibrium

Owing to an increase in the electron number density in the plasma due to ionization of argon, the equilibrium would shift toward the neutral atom species resulting in enhancement of atomic emission and depression in ionic emission. In this case, the rate of electron-ion recombination increases in the presence of interfering element [8]. The degree to which this mechanism will influence emission intensities in the plasma will depend on how much the electron number density is changed by introduction of the EIE [8].

1.3.4.1 (h) Volatilization effects

Volatilization effects may be relevant in the presence of EIEs [31]. In this mechanism, the analyte atoms are 'included' in a desolvated particle matrix which may take longer to volatilize than analyte particles alone. This may either be the result of larger particles, or particles with atomic bonds which are more difficult to break. The net effect is a delay in the release of the analyte atoms, when compared to the situation without matrix. This delayed vaporization can result in the spatial behaviour of analyte emission.

1.3.5 Steady-state rate model

Several authors have applied steady-state kinetic equations using the classical reaction rate model to describe the excitation processes in the plasma [50, 95, 100, 101, 102, 126]. Lovett [147] itemized many of the possible single step reactions possible for analytes in an argon ICP and applied the steady-state approximation to each of the alkaline earth elements, with a system including about 100 atomic levels of an alkaline earth element and several for argon, both

atomic and ionized. He presented a quantitative model of the ICP excitation utilizing the individual rates for all processes, which excite, de-excite, ionise, or recombine the analyte atom or ion. The following processes were considered in the kinetic scheme [147]:

(i). Collisional excitation:
$$X_p + e^- \longrightarrow X_q$$
 (21)

(ii). Collisional decay:
$$X_q + e^- \longrightarrow X_p + e^-$$
 (22)

(iii). Collisional ionisation:
$$X_p + e^- \longrightarrow X_c^+ + 2e^-$$
 (23)

(iv). Three body recombination:
$$X_c^+ + 2e^- \longrightarrow X_p + e^-$$
 (24)

(v). Radiative recombination:
$$X_c^+ + e^- \longrightarrow X_p + hv$$
 (25)

(vi). Autoionization:
$$X_q^* \longrightarrow X_c^+ + e^-$$
 (26)

(vii). Radiative decay:
$$X_q^* \longrightarrow X_p + h\nu$$
 (27)

(viii). Penning ionisation:
$$Ar^m + X_p \longrightarrow X_c^+ + Ar + e^-$$
 (28)

In these processes, level p>q.

The following equations were proposed for estimation of various rate constants *a priori* for processes occurring in the plasma;

1.3.5 (a) Collisional excitation rate constant [147]:

$$X_{p} + e^{-} \rightarrow X_{q} + e^{-}$$
 (29)

$$R_{CE} = 1.58 \times 10^{-5} [f_{pq} < \overline{G}_{pq} > /\chi T_e^{1/2}] \exp(-\chi/T_e) n_e = K_{ce} (q, p) n_e$$
 (30)

where, $\underline{\chi}$ = transition energy (eV) $<\overline{G}_{pq}>$ = thermally averaged Gaunt factor oscillator strength

1.3.5 (b) Collisional Ionization rate constant [147]:

$$X_p + e^- \longrightarrow X_c^+ + 2e^-$$
 (31)

$$R_{CI} = 1.24 \times 10^{-6} \xi T_e^{-3/2} [\exp(-\varphi/\varphi^2)][0.915(1 + 0.64)/\varphi)^{-2} + 0.42(1 + 0.5/\varphi)^{-2}]n_e = K_{CI}(c,p)n_e$$
(32)

where $\varphi = E_i/T_e$ $\xi = \text{number of ionizable electrons.}$

1.3.5 (c) Three-body recombination rate constant [147]:

$$X_c^+ + 2e^- \longrightarrow X_p + e^-$$
 (33)

$$R_{3b} = R_{Cl} n_e / 6.037 \times 10^{21} \text{ g/g}_p T_e^{3/2} \exp(-\chi / T_e) = k_{3b}(p,c) n_e^3$$
(34)

where R_{Cl} is the rate for collisional ionization.

1.3.5 (d) Radiative recombination rate constant [147]:

$$X_c^+ + e^- \longrightarrow X_p + h\nu \tag{35}$$

$$R_{rr} = 5.2 \times 10^{-14} (Z + 1) \phi^{1/2} (0.43 + 0.5 \ln \phi + 0.47 \phi^{-1/3}) n_e$$

$$= k_{rr}(p,c) n_e$$
(36)

where Z is the charge on the recombined species.

Lovett used his model to assess the effect of the various processes (described above) on the level of populations of analyte atoms and related the effects to possible changes in temperature and electron number density. This approach applied input temperature and electron number density, i.e assuming an LTE backbone. Therefore the fact that Lovett uses a single temperature for all reactions and, furthermore, uniform, high values for both temperature (8 200K) and the electron number density (3.34 x 10^{15} cm⁻³) makes his approach less applicable to practical ICP analysis. By assuming that the temperature that controls the reaction rate constants for the forward and reverse reaction was the same, the local thermodynamic equilibrium (LTE) condition is implied in the model. The calculated population densities, assuming $T_e = 8200$ K and $n_e = 3.34$ x 10^{15} cm⁻³,

showed very close values to LTE for atomic levels and slight under-population for ionic levels, which disagreed with experimental results previously reported [148], i.e. overpopulation of ions. de Galan [114] suggested that these minor deviations from LTE were due to the relatively high values of T_e and n_e . However, it is now widely accepted that the ICP is not in local thermal equilibrium [95]. Accordingly, experimental values of T_e and n_e are essential for the collisional-radiative model. Another limitation of Lovett's approach is that the reported data do not refer to the region of interest, the normal analytical observation zone. However, the merit of the case presented in the paper is that it does demonstrate that under conditions of high temperature (8 200 K) and high electron number density (3 x 10^{15} cm 3) the induction region is close to thermal equilibrium although such conditions do not prevail in the normal analytical observation zone.

Goldwaser and Mermet [148] investigated charge transfer processes between argon and analyte, considering several electronic states and applied the steady-state approximation. Furthermore, Hasegawa and Haraguchi [117] incorporated ambipolar diffusion and convection into the rate model and applied it to magnesium and cadmium analytes. The authors made a brave attempt to estimate rate constants *a priori* for the processes they considered to be significant. Some of the expressions are itemised below:

1.3.5 (e) Electron impact excitation and de-excitation rate constant [117].

$$Ar(p) + e^{-} \Leftrightarrow Ar(q) + e^{-}; k_{pq}, k_{qp}$$
 (37)

$$k_{pq} = \frac{1}{\sqrt{me}} \left(\frac{2}{\pi k T_e}\right)^{3/2} \int_{Epq}^{\infty} (E) e^{-E/kTe} dE$$
 (38)

where Ar(p) is the argon atom in the level p, and k_{pq} and k_{qp} are the rate coefficients for electron impact excitation from level p to q and de-excitation from q to p, respectively, m_e = electronic mass, k the Boltzman constant, E the incident energy of the electron, E_{pq} the energy difference between states p and q, Q_{pq} (E) the excitation cross-section from p to q.

1.3.5 (f) Ionization and three-body recombination rate constant [117]:

$$Ar(p) + e^{-} \underset{k_{in}}{\overset{k_{pi}}{\Leftrightarrow}} Ar^{+} + 2e^{-}$$
(39)

$$k_{ip} = k_{pi} \left(\frac{h^2}{2\pi m_e k T_e} \right)^{3/2} \frac{g_p}{2g_i} \exp\left(\frac{E_{pi}}{k T_e} \right)$$
 (40)

where k_{pi} and k_{ip} are rate constants for electron impact ionization and three-body recombination, respectively.

The authors found out that for atmospheric pressure argon ICP, the calculated population densities suggested an overpopulation of lower argon states and the approach to local thermal equilibrium at higher n_e [117]. The mechanism they derived involved collisional excitation. For low lying states, spontaneous emission is dominant and balanced with collisional excitation from the lower states. This results in an overpopulation of lower states, especially the ground state. On the other hand, the upper levels are closer to LTE due to the dominated collisional excitation and de-excitation from the adjacent states.

However, a limitation to this approach, as noted by the authors, is the scarcity of theoretical or experimental data for $Q_{pq}(E)$, which are limited to excitation from the ground state. Further precise measurements of the spatial

distribution of various parameters would be required in order to evaluate the mechanism [117].

Steady-state treatment by Hieftje *et al.* [95], using the classical equations generated the following kinetic rate expressions for the four major analyte species (the ground state atom, the excited-state atom, the ground-state ion, and the excited-state ion):

$$\frac{d[M]}{dt} = A_2[M^*] + k_8[M^+][e^-] + k_9[M^{**}][e^-] + k_{17}[M^*][e^-]
+ k_{11}[M^+][e^-]^2 + k_{13}[M^{**}][e^-]^2 - k_1[M][Ar^*]
- k_7[M][Ar^*] - (k_3 + k_5 + k_6)[M][e^-]$$
(44)

$$\frac{d[M^*]}{dt} = k_2[M^+][e^-] + k_3[M][e^-] + k_{10}[M^{+*}][e^-] + k_{12}[M^+][e^-]^2
+ k_{14}[M^{+*}][e^-]^2 - A_2[M^*] - (k_{15} + k_{16} + k_{17})[M^*][e^-]$$
(45)

$$\frac{d[M^{+}]}{dt} = A_{1}[M^{+*}] + k_{5}[M][e^{-}] + k_{7}[M][Ar^{*}] + k_{15}[M^{*}][e^{-}]
+ k_{18}[M^{+*}][e^{-}] - (k_{2} + k_{4} + k_{8})[M^{+}][e^{-}]
- (k_{11} + k_{12})[M^{+}][e^{-}]^{2}$$
(46)

$$\frac{d[M^{+*}]}{dt} = k_1[M][Ar^*] + k_4[M^+][e^-] + k_6[M][e^-] + k_{16}[M^*][e^-]
- A_1[M^{+*}] - (k_9 + k_{10} + k_{18})[M^{+*}][e^-]
- (k_{13} + k_{14})[M^{+*}][e^-]^2$$
(47)

Clearly, when steady state treatment is applied to equations (44-47), the complexity of the resulting relationships is formidable. Each of the two resulting expressions involves eight separate terms with coefficients involving as many as 13 different rate constants. Needless to say, the difficulty in interpreting the meaning of such complex terms, even when correlation exists, might nullify the treatment [95]. In addition, correlations which are observed for one metal might not exist for another. Accordingly it would be necessary to produce a complete set of

the various spatial profiles for each analyte to be investigated. In light of this background, some workers have opted to use simplified reaction rate models to study the effects of EIEs in the ICP.

1.3.6 Simplified reaction rate model

The simplified reaction rate model approach has been used by Zaranyika et al [100-102, 126] and Hieftje et al, [14, 50, 127, 128] to model the effects of EIEs in the ICP.

The approach by Hieftje and co-workers exploits the heterogeneous spatial character of the plasma as a means of distinguishing among apparently viable mechanisms [14, 50, 52-60, 127, 128]. Under steady-state conditions, each excitation model predicts proportionality between atomic or ionic emission and localised concentrations of species involved in the excitation process. As a result, models can be tested by comparing spatial emission behaviour with experimental maps of reactant concentration and partners (or products of such maps) which the model assumes are important. Generally, a specific mechanism of excitation or ionisation is first proposed and corresponding steady-state kinetic expression developed. This hypothesis is then tested through the use of the derived steady-state relationships and appropriate experimentally developed parameters and spatial maps. Assuming that excited-state species can relax either radiatively [50, 95]:

$$M^{+*} \xrightarrow{A_1} M^+ + hv_i \tag{48}$$

$$M^* \xrightarrow{A_2} M + hv_a \tag{49}$$

or through inelastic collision with an unbound electron [65]:

$$M^{+*} + e^{-} \xrightarrow{k_{ci}} M^{+} + e^{-}$$
 (50)

$$M^* + e^{-} \xrightarrow{k_{ca}} M + e^{-} \tag{51}$$

and also assuming that analyte ionization and excitation can also occur by a Penning process, which can be represented as [50, 95]:

$$M + Ar^m \longrightarrow M^{+*} + Ar + e^- \tag{52}$$

where Ar^m designates an Ar atom excited to a metastable state, but can also denote other excited Ar atoms with sufficient energy to generate an excited-state analyte ion, according to Rayson and Hieftje [50]. If it is assumed that reaction (51) could yield with equal probability a ground-state ion, then Eqns (50), (51) and (52) can be combined to from equation the following equation [50, 95]:

$$\frac{d[M^{+*}]}{dt} = k[M[Ar^{m}] - A_{1}[M^{+*}] - k_{ci}[M^{+*}][e^{-}]$$
(53)

Under steady-state conditions, Eqn (53) can be further simplified by its division into two separate cases involving, respectively, the dominance of radiative or collisional deactivation as energy loss processes. This dominance could be dictated by the relative magnitudes of A_1 and the product $k_{ci}[e^-]$ [50]:

(i). Dominance of radiative decay mechanism.

$$[M^{+*}] = (k / A_1)[M][Ar^m]$$
(54)

(ii). Dominance of collisional deactivation.

$$[M^{+*}] = \frac{k[M][Ar^m]}{k_{ci}[e^-]}$$
 (55)

The relative impact of the proposed processes on excitation in the analytical ICP can then be investigated using experimentally obtained measurements. The relationships described above predict direct (linear) correlation to exist between the analyte emission signal and number density of one or more species within the plasma. Thus, the existence of a predicted correlation might indicate a specific mechanism to be significant for excitation of the analyte and also, the lack of such a linear correlation would suggest that the selected mechanism is at most a minor contributor to excitation. When applied to the above processes, a direct correlation between analyte ion emission intensity and the product function $(k \, / \, A_{\!\scriptscriptstyle 1})[M\,][Ar^{\,\scriptscriptstyle m}\,]$, would suggest that radiative decay is a significant process, whereas high correlation between analyte ion emission intensity and the product function $\frac{k[M][Ar^m]}{k_{x}[e^-]}$ would suggest that collisional deactivation is a dominant mechanism. When the approach is applied to excitation of calcium, the authors concluded that a high a localised concentration of ground-state Ca atoms in the central channel of the ICP appeared to swamp any proposed mechanism in which it would be involved [50]. As a result, both Ca atom and ion excitation seemed independent of Ca atom concentration. Three-body and radiative recombination processes appeared to be most significant in Ca excitation, whereas Ca ion excitation seemed to occur principally by direct electron impact.

More recently Hieftje *et al.* [128-131] have reported a simplified steady-state approach utilising a suit of sophisticated experimental equipment. The following kinetic experiments were considered for dominance, during the determination of calcium by ICP.

(a). Ion-electron re-combination to excited state followed predominantly by radiative decay to ground state [14]:

$$Ca^{+} + e^{-} \xrightarrow{k_{1}} Ca * \tag{56}$$

$$Ca * \xrightarrow{k_2} Ca + hv \tag{57}$$

(b). Electron impact excitation followed predominantly by radiative decay to ground state [14]:

$$Ca + e^{-} \xrightarrow{k_3} Ca * + e^{-}$$
 (58)

$$Ca * \xrightarrow{k_4} Ca + hv \tag{59}$$

Assuming steady state at any location in the plasma (an assumption apparent from the fact that emission from any volume element is stable), then the following rate expressions can be developed for the above processes [14]:

d [Ca*] / dt =
$$k_1$$
 [Ca*][e-] - k_2 [Ca*] = 0
Therefore [Ca*] = (k_1 / k_2) [Ca*][e-] (60)

Therefore this mechanism would predict a direct proportionality between Ca^* (and therefore Ca^* atom emission) and the product of the Ca^* ion ground state concentration and the electron concentration in every volume element of the plasma. In (b), a direct proportionality between Ca atom ground state concentration and the electron concentration in every volume element of the plasma would be predicted. This treatment requires that k_1 , k_2 , k_3 and k_4 be constant, and hence applies to the isothermal zones in the discharge. For every reasonable mechanism for both atomic and ionic lines, correlation plots have been developed between the

parameters indicated by each equation; those with the best linearity then taken as the most likely candidates for the prevailing mechanism. From these studies, Hieftje et al have concluded that calcium atoms appear to follow the mechanism in (a) above, whereas calcium ions appeared to be excited by electron impact, but deactivated principally through radiative decay. However, the authors have concluded that a great deal still remains unknown about the analytical ICP and the events that occur in it. Further work is still needed to establish a clearer understanding of how sample atomisation, how atoms and ions are formed and excited, and how inter-element interferences arise, in order to have hope of overcoming the matrix interferences in a rational way.

Zaranyika *et al.* [100-102, 126] have used simplified reaction rate models which focus on only one particular electronic level for the effect of EIEs in the airacetylene flame and the ICP. Along with the simplified models, they proposed a novel method for probing changes in the number density of the analyte excited state, n_u , based on determining the analyte emission (E) signal ratio E'/E, where the prime denotes presence of interferent, and comparing to theoretical values derived assuming a simplified rate model based on steady state kinetics in the plasma. The approach assumes no change in the rate of introduction of analyte atoms into the excitation source, and no change in the temperature of the torch or flame, upon the simultaneous introduction of an easily ionized interferent element. The argument by the authors is that according to the LTE approach, atomic line absorption and atomic line emission intensities are directly proportional to the population of the ground and excited states, respectively, i.e., $A \propto N_0$ and $E \propto N_j$, where A is the absorption signal intensity and E is the line emission signal

intensity, and N_0 and N_j are the atomic populations of the ground and excited states, respectively. N_i and N_0 are related by the Boltzmann equation [17, 39]:

$$N_{j} = N_{o} \left(\frac{g_{j}}{g_{o}} \right) \exp(-\Delta E / kT)$$
 (61)

where g_j and g_0 are the statistical weights of the excited and ground states, respectively, k is the Boltzmann constant, T is the absolute temperature and ΔE is the difference in the energies of the two electronic states involved in the transition.

If the rate of introduction of the analyte atoms into the plasma is kept constant, and we assume no change in the plasma temperature on simultaneous introduction of interferent metal atoms with the analyte, we may write [100-102]:

$$N_{j}' = N_{o}' \left(\frac{g_{j}}{g_{o}}\right) \exp\left(-\Delta E / kT\right)$$
 (62)

where the primes denote the actual populations of analyte excited atoms in the presence of the interferent. Combining equations 61 and 62, we have

$$\frac{N_j'}{N_j} = \frac{N_o'}{N_o} \tag{63}$$

Hence,

$$\frac{E'}{E} = \frac{A'}{A} = \frac{n_u'}{n_u} \tag{64}$$

Equation 64 suggests that the effects of collisional processes on the excitation, ionization and line emission of the analyte atoms resulting from the presence of interferent atoms may be followed by measuring the absorption or emission intensities of a given concentration of analyte atoms in the absence and presence of the interferent, and comparing the E'/E and A'/A ratios plotted versus analyte concentration. Applying the approach to emission spectrometry, the following situations may be identified [100-102]:

- (i). No collisional effects, and therefore no change in the populations of the ground and excited states of analyte atoms: E'/E=1
- (ii). Increase of ground state, e.g. suppression of ionization: E'/E>1
- (iii). Depopulation of ground state, e.g. charge transfer reactions: E'/E<1
- (iv). Increase in excited state population: E'/E>1
- (v). Depopulation of excited state: E'/E<1

Therefore by plotting theoretical curves of n_u'/n_u as a function of analyte concentration and comparing the curves with the experimental E'/E, the processes which perturb the excitation mechanism of the analyte species may be deduced. On applying the simplified reaction rate model to the effects of excess Na on emission of K during air-acetylene flame emission spectrometry [100], the authors found out that their results confirmed overpopulation in terms of the Boltzman equation, of the excited state as a result of collisional excitation. When observations were made from the primary reaction zone of the flame, overpopulation of the ground state was also observed. The results were explained in terms of a steady state kinetic model which takes into account collisional excitation and collisional charge transfer, in addition to thermal excitation, thermal ionization and radiative de-excitation processes within the flame.

On applying the simplified approach to the effects of excess Li on Ca in the ICP, Zaranyika and Chirenje [126], proposed the kinetic scheme shown in figure 2. The model took into account (a) the relative rates of thermal dissociation of analyte salt, (b) collisional recombination of counter atom and analyte atoms, (c) charge transfer between analyte and argon species and (e) ion/electron collisional recombination.

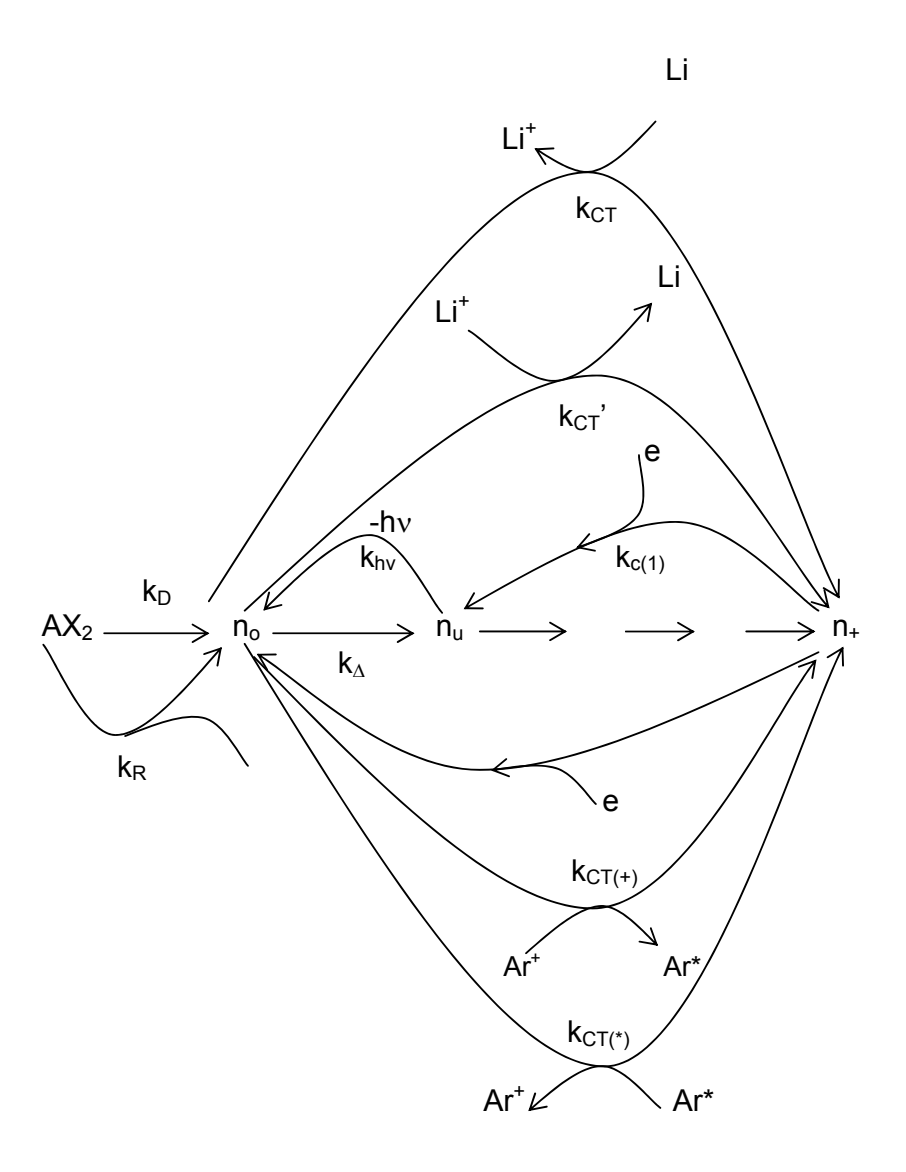


Fig.2. Schematic representation of the model proposed by Zaranyika et al. [126].

n denotes number density, the subscripts o, u, +, AX_2 , X, m_o , and m_+ denote analyte ground state, analyte excited state, analyte ion, analyte salt, counter atom, ground state interferent atom and interferent ion, respectively; Ar(*) and Ar(+) denote argon excited state and ions, respectively; the prime in n_u , n_e and n_x denotes quantities measured in the presence of the interferent; k_D is the rate constant for thermal dissociation, k_A is the rate constant for thermal excitation from ground state; $k_{c(0)}$ is the rate constant for ion-electron collisional recombination to the ground state; $k_{(c1)}$ is the rate constant for ion-electron collisional recombination to the first excited state; k_{CT} and k_{CT} are the rate constants for collisional charge transfer involving Li species; $k_{CT(*)}$ and $k_{CT(*)}$ are the rate constant for collisional charge transfer involving argon species; k_R is the rate constant for collisional recombination of analyte and counter atoms.

Assuming a steady state with respect to the number density of analyte ground state atoms, n_0 , and analyte excited state atoms, n_u , it can be shown that the ratio of the number density of analyte atoms in the excited state in the presence of the interferent, n_u , that in the absence of interferent, n_u , is given by:

$$\frac{n_{u}'}{n_{u}} = 1 + \frac{\left[(1 - f_{m}) \alpha_{1} k_{CT} n_{+} n_{m(0)} - (1 - f_{n}) \gamma_{1} k_{R} n_{0} \Delta n_{X} - (1 - f_{n}) \gamma_{2} k_{CT}' n_{0} n_{m(+)} \right]}{\left[(1 - f_{a}) k_{D} n_{AX_{2}} + \alpha_{2} k_{CT(*)} n_{+} n_{Ar(*)} + \beta_{0} k_{c(0)} n_{+} n_{e} + \beta_{1} k_{c(1)} n_{+} n_{e} \right]}$$

$$(65)$$

where n denotes number density, the subscripts o, u, +, AX_2 , X, m_o , and m_+ denote analyte ground state, analyte excited state, analyte ion, analyte salt, counter atom, ground state interferent atom and interferent ion, respectively; Ar(*) and Ar(+) denote argon excited state and ions, respectively; the prime in n_u , n_e and n_x denotes quantities measured in the presence of the interferent; k_D is the rate constant for thermal dissociation, k_A is the rate constant for thermal excitation from ground state; $k_{c(0)}$ is the rate constant for ion-electron collisional recombination to the ground state; $k_{(c1)}$ is the rate constant for ion-electron collisional recombination to the first excited state; k_{CT} and k_{CT} are the rate constants for collisional charge transfer involving Li species; $k_{CT(1)}$ and $k_{CT(+)}$ are the rate constant for collisional charge transfer involving argon species; k_R is the rate constant for collisional recombination of analyte and counter atoms; α , β , and γ are the fraction of analyte ions undergoing collisional charge transfer interactions, the fraction of analyte ions undergoing collisional ion-electron recombination, and the fraction of analyte ground state atoms undergoing collisional charge transfer interactions,

respectively, and f_a , f_n and f_m are the analyte salt fraction atomized, analyte fraction ionized, and interferent fraction ionized, respectively.

The degree of ionization was calculated using the Saha equation [39]:

$$\frac{n_3}{n_1} = \frac{6.037 \times 10^{21}}{n_e} \cdot \frac{g_3}{g_1} \cdot T_e^{3/2} \cdot \exp\left\{-\left(E_3 - E_1\right)/T_e\right\}$$
(66)

or

$$Log\left(\frac{N_{+}N_{e}}{N_{0}}\right) = -\alpha.\Phi - \frac{3}{2}\log\Phi + 20.9366 + \log\left(\frac{2U_{+}}{U_{0}}\right)$$
 (67)

where α = ionization potential

 $\phi = 5040 / T$

U = partition function

N = number density

and the subscripts 0, + and e denote the ground state, ion and electron respectively.

For Ca and Li, the values obtained were in excess of the ground state number densities implying approximately 100% ionization. As near 100% ionization implies near 100% atomization, in equation 65, f_a =1, f_n = 1, and f_m = 1, i.e., the contribution of thermal dissociation, Ca/CI collisional recombination, and all the terms containing n_{AX} , n_o and $n_{m(o)}$, become negligible. The rate constants $k_{CT(^*)}$ and $k_{c(1)}$ were calculated assuming collision theory and Arrhenius equation respectively, and on this basis, it was shown that $k_{CT(^*)} << k_{c(1)}$. It was also shown that $k_{c(o)} << k_{c(1)}$ and $\beta_o << \beta_1$. Under these conditions, equation 65 reduced to [126]:

$$\frac{n_{u}'}{n_{u}} = 1 + \frac{\beta_{1}k_{c(1)}n_{+}n_{m+}}{\alpha_{2}k_{CT(*)}n_{+}n_{Ar(*)} + \beta_{1}k_{c(1)}n_{+}n_{Ar(+)} + \beta_{1}k_{c(1)}(n_{+})^{2}}$$
(68)

As $n_{Ar(*)} \ll n_{Ar(*)}$, and assuming $\alpha_2 \ll \beta_1$, equation 68 further reduced to

$$\frac{n_u'}{n_u} = 1 + \frac{n_{m(+)}}{n_{Ar(+)} + n_+} \tag{69}$$

The experiment was designed such that n_{m+} is constant, and n_+ was varied.

Since $n_{Ar(+)} >> n_{m(+)} >> n_+$, suggesting that the value of n_u'/n_u should be a constant approximately equal to unity for all values of n_+ . This was contrary to experiment as shown in Fig. 3. The authors attributed this to the fact that only a small fraction of electrons from the ionization of Ar were involved in collisions with analyte ions, while the bulk of these electrons were involved with Ar species. However, no detailed explanation was given by the authors for the suggestion. The authors showed statistically this to be the case. The results suggested that the contribution of collisional recombination involving electrons from the ionization of Ar to the observed interferents effects was negligible under these conditions, and equation 69 reduces to [126]:

$$\frac{n_u'}{n_u} = 1 + \frac{n_{m(+)}}{n_+} \tag{70}.$$

Equation 70 gave a curve similar to the experimental curve. Numerical results above 1 ppm analyte concentration were in good agreement with experiment, but results below 1 ppm were up to 2 orders of magnitude higher than experiment. The authors attributed this to three factors; (a) collisional de-excitation

of excited analyte atoms which had not been taken into account in the formulation of the model, (b) that only a fraction of electrons from the ionization of interferent were involved in collisional recombination to give analyte excited state atoms, (c) collisional ionization of analyte excited state atoms. When these were factored into eq. 70, eq. 70a was obtained [126]:

$$\frac{n_u'}{n_u} = 1 + \frac{(1 - \chi_{m+})n_{m+}}{n_+} \left[\frac{\delta'}{\delta} \right]$$
 (70a)

Where χ_{m+} = fraction of electrons from the ionization of the interferent undergoing collisions with interferent species, and [126]:

$$\frac{\delta'}{\delta} = \frac{k_{hv} + k_{CD}n_e + k_{CI}n_e}{k_{hv} + k_{CD}n'_e + k_{CI}n'_e}$$
(70b)

Where k_{CD} and k_{CI} are the rate constants for collisional de-excitation and collisional ionization, respectively. Simulation of the experimental curve using eq. 70a after evaluation of the statistical factor χ_{m+} and evaluation of the rate constants k_{CD} and k_{CI} using the Grossdover formula for estimating the collisional cross-section for electronic collisions [126], gave theoretical E'/E curves similar in shape to the experimental curves and coincided with the experimental curves at high concentrations, but were up to 2 orders of magnitude higher than the experimental curves below about 10 μ g/mL Ca concentration in the test solution.

The work by Zaranyika and Chirenje resulted in some important findings [126]:

- That it is possible to simulate the effects of EIEs on analyte emission in the ICP.
- 2. The results of their modelling lead to some important conclusions regarding the mechanism of interference resulting from the presence of interferent. These are:
 - (a). That contributions from charge transfer between analyte and interferent species, and between analyte and argon species were negligible.
 - (b). That the contribution of thermal excitation was negligible.
 - (c). That the observed interference effects could be attributed to ionelectron collisional recombination.
 - (d). That not all the electrons from the ionization of the interferent EIE were involved in collisional effects leading to excitation of analyte.
 - (e). That electrons from the ionization of Ar were not involved in collisional processes leading to the observed emission signal enhancement.
 - (f). That collisional de-excitation reduced the signal enhancement considerably.

The major conclusion from the work by Zaranyika and Chirenje relates to the apparent non-participation of electrons from the ionization of Ar, or the apparent non-involvement of Ar species, in the collisional excitation of the analyte during ICP-OES. If this is indeed the case, and cognisance is taken of the fact that temperature appears both in the numerator and denominator of equation 70a, then

we would expect that the interference effects of EIEs on analyte emission will be similar in the ICP and Flame systems. Thus a comparative study of the effects of EIEs in ICP and flame systems should provide confirmation or otherwise of the apparent non-involvement of electrons from the ionization of Ar, or the apparent non-involvement of any other Ar species in the collisional excitation of the analyte in ICP systems.

The lack of absolute agreement between experiment and theory as represented by eq. 70a can be attributed to the difficulties inherent in estimating the value of the statistical factor χ_{m+} , and estimating the values of the rate constants k_{CD} and k_{Cl}. The Gross Dover equation was designed for estimating the cross-section for collisional ionization from the ground state by electrons, and may not be adequate for the estimation of the cross-section for collisional de-excitation, or collisional ionization from the excited state [149]. Assuming that the conclusion relating to the non-involvement of electrons from the ionization of Ar is confirmed, the second aim of the present work will be to investigate the experimental determination of the collisional de-excitation rate constant, and the use of such impirical rate constants in simulating interference effects off EIEs during ICP-OES. The model proposed by Zaranyika and Chirenje did not take into account collisional excitation. Blades and Horlick, [31, 150] have suggested that collisional excitation is a significant process in explaining the effects of EIEs on analyte emission signal. Thus in this work the kinetic model proposed by Zaranyika and Chirenje will be modified to take into account collisional de-excitation of analyte excited state as well as collisional excitation of analyte atoms or ions.

The other major conclusion made by Zaranyika and Chirenje was that charge transfer between analyte and interferent species was negligible. This

conclusion related to charge transfer between analyte ion and interferent ground state or vice versa. Charge transfer between analyte ion and activated interferent atoms was evaluated only for Ar as the interaction species. Gunter *et al.* [42] suggested that charge transfer reactions were responsible for the rise in excited state of calcium species. The third aim of the present work will be to evaluate the possibility of collisional excitation of analyte via collisional charge transfer between analyte ions and activated interferent species.

Aims:

- (a) To carry out a comparative study of the effects of EIEs on analyte emission signal enhancement during ICP and flame AES, with a view to confirm or otherwise, the non-involvement of Ar species in collisional excitation of analyte during ICP-OES. This will be covered in Chapter 2 of this dissertation.
- (b) To investigate the applicability of the charge transfer and ambipolar diffusion models to account for the emission signal enhancement in during ICP-OES and flame AES. This will be covered in Chapters 3 and 4 of this dissertation respectively.

Specific objectives

(a) To obtain emission intensity data for Ca(II), Mg(II) and Sr(II) in the absence and presence of excess K and Li as interferents during ICP-OES determination and for K(I) and Mg(I) in the absence and presence of Na and K in flame AES respectively.

- (b) To formulate kinetic equations for the charge transfer and ambipolar diffusion models for the proposed excitation processes.
- (c) To explore the possibility of predicting the experimental calibration curve using the charge transfer and ambipolar diffusion models.

CHAPTER 2

EXPERIMENTAL COMPARATIVE STUDY OF THE EFFECTS OF EASILY IONIZED ELEMENTS ON ANALYTE LINE EMISSION DURING ICP AND AIR-ACETYLENE FLAME EMISSION SPECTROMETRY

2.1 Composition of the ICP torch and Air-acetylene flame

The rationale for the comparative study of the effects of EIEs in the ICP and Flame systems was discussed above. However, for a fuller understanding of why, in the event that the non-involvement of Ar species in the collisional excitation of analyte in the ICP, we would expect the effects of EIEs to be similar in the ICP and flame systems, it is necessary to give a brief description of the composition of the plasma in ICP and flame systems. The ICP torch was described in Section 1.1 above. Reference to Fig. 1 shows that the plasma in the ICP will be composed of particles derived from Ar and sample solution. The sample solution often consists of water, an acid used to stabilize the solution (usually HCI), and analyte salt (or organic complex). For the experiments envisaged in the present study, the sample solution consisted of water, HCI and analyte chloride salt. The plasma in the analytical zone of the torch will be composed of the following:

Table 1. Composition of the analytical zone plasma in the ICP

Source	Atoms	Excited	lons	Electrons
		atoms		
Argon	Ar	Ar*	Ar ⁺	e ⁻
Water	O, H	O*, H*	O⁺, H⁺	e ⁻
HCI	H, Cl	H [*] , Cl [*]	H ⁺ , Cl ⁺	e ⁻
MCI	M, CI	M [*] , Cl [*]	M ⁺ , CI ⁺	e ⁻

In flame atomic spectrometry, the flame is generated using a fuel gas and an oxidant gas. In air-acetylene flame spectrometry, acetylene is the fuel and air the oxidant gas to give a flame of about 2573 K in the analytical zone. If the sample solution is dilute HCl solution, then the particles in the analytical zone of an air-acetylene flame will be as shown in Table 2. Note that because of the lower temperature of the flame, plasma will contain molecular species, in addition to atomic species and free electrons.

Table 2. Flame composition in Air-acetylene flame spectrometry

Source	Atoms	Excited	lons	Electrons	Molecules
		atoms			
C ₂ H ₂	C, H	C [*] , H [*]	C ⁺ , H ⁺	e ⁻	CH, H ₂
Air	O, N, etc	O*, N*	O ⁺ , N ⁺	e ⁻	O ₂ , N ₂ , NO
Water	O, H	O*, H*	O⁺, H⁺	e ⁻	O ₂ , OH, H ₂
HCI	H, Cl	H [*] , Cl [*]	H ⁺ , Cl ⁺	e ⁻	H ₂ , Cl ₂ , etc
MCI	M, Cl	M [*] , CI [*]	M ⁺ , CI ⁺	e ⁻	M ₂ , MO,
					MCI, MC,

Collisional excitation involves transfer of energy or electrons to analyte species, and can only result from:

- (a). Electron impact excitation
- (b). Ion-electron radiative recombination, or
- (c). Charge transfer involving analyte ions and activated interferent atoms.

Oxygen, hydrogen and carbon all have very high ionization energies, hence they are ionized to small extents in the air-acetylene flame. In addition, because of their high ionization potentials, they require high energies in order to excite them in sufficient quantities to impact on analyte excitation via analyte-ion/activated-interferent-atom charge transfer. Thus if Ar species in the ICP are not involved in collisional excitation, then the situation in the ICP becomes similar to that in the air acetylene flame.

2.2 Methodology

The comparative study of the effects of EIEs on analyte line was carried out by generating line emission intensity data for interferent-spiked and un-spiked analyte standard solutions using Flame AES and ICP-OES. In order to minimize changes in the physical properties of the test solution upon introduction of interferent, the interferent concentration was constant at a very high level (1000 mg/L) relative to that of the analyte (0-30 mg/L), whilst the analyte concentration was varied. Preliminary experiments were carried out to determine the aspiration rate and nebulization efficiency for the solutions under analysis. Experimental E'/E ratios were calculated and plotted Vs analyte concentration for comparison.

2.3 EXPERIMENTAL

2.3.1 ICP equipment

A Spectroflame Modula 90/95 Inductively Coupled Argon Plasma Echelle Spectrophotometer (supplied by SPECTRO Analytical Instruments, GmbH, Boschstrabe, Germany) was used. The spectrophotometer was fitted with an aperture plate of 90 mm by 1.5 nm slits etched at 2 mm intervals, a photomultiplier

tube (PMT) detector mounted on a movable frame for radial view of the ICP, a torch with three concentric tubes for outer gas, auxiliary gas and sample transport, a free running 40.68 MHz R.F generator with a power supply varying from 0.5 to 2 kW, a 5-channel computer controlled peristaltic pump, and an automatic Ar gas flow rate optimizer. The generator operated at 1.2 kW power.

The argon (99.998 %) was supplied from a pressurised tank (Afrox Ltd, South Africa). The maximum impurities specified were: $O_2 - 3$ ppm; moisture - 3 ppm; $N_2 - 14$ ppm. The outer gas was supplied at 14 Lmin⁻¹, nebulizer pressure 40 psi (280 KPa) and auxiliary gas at 1 Lmin⁻¹. Under these conditions the excitation temperature was ranged between 7000 and 9000 K [151]. The instrument was optimised using a 100-mg/L solution of Mn. The strong emission of Mn line was used to establish the optimum zone for analysis. The maximum temperature of 9000 K was used in the calculations for maximum effect of the interferent.

2.3.2 Flame equipment

Flame experiments were run using a Shimadzu AA – 6701 Flame Atomic Absorption/Emission Spectrometer fitted with a high resolution Czerny-Turner monochromator, automatic baseline drift correction using electrical double beam signal processing, and an air-cooled premix type 100 mm single slot burner with a stainless steel head, Pt-Ir capillary nebulizer with Teflon orifice, glass impact bead and polypropylene chamber. The spectrometer was coupled to an ASC-6100 Shimadzu Auto Sampler. The air was supplied by an Atlas Copco air compressor (ETS SESCA, France) at 350 KPa input pressure, while the fuel gas, acetylene, was supplied from a pressurised tank (Oxyco Zimbabwe, Harare) at 1000 Kpa. The spectrophotometer was fitted with an automatic fuel gas flow rate optimization for

each element to be measured. Optimum air-acetylene gas flow rates for K and Mg were 2.0 and 1.8 L/min. Under these conditions the temperature of the flame was 2573 K (Shimadzu AA – 6701 user manual). Other instrumental settings employed were as follows: wavelength 766.5 nm and 285.2 nm for K and Mg respectively, slit width 0.1 nm, burner height 7 mm, burner angle 0°, secondary acetylene gas pressure 90 Kpa, pre-spray time 3s, integration time 5s and response time 1s.

2.3.3 Materials

The following material were used: Calcium chloride, magnesium chloride, strontium chloride, lithium chloride, potassium chloride and sodium chloride, all AR grade; De-ionised water of conductivity $0.002~\mu S$.

2.3.4 Procedure

The procedure used was the same as the one used by Zaranyika and coworkers [100-102, 126]. Two sets of standard solutions containing 0 to 30-mg/L analyte (Ca, Mg, Sr or K) were prepared from freshly prepared solutions of their chloride salt solutions. One set was spiked with 1000 mg/L of interferent (Li, K or Na) also prepared from the chloride salt. The other set was left unspiked. In order to minimise changes in the physical properties of the test solution upon the introduction of the interferent, the interferent concentration was kept constant at a very high level (1000 mg/L) relative to that of the analyte (0 –30 mg/L), whilst the analyte concentration was varied. Under these conditions any effect due the to changes in the physical properties of the test solution in going from the interferent-free solution to the interferent-spiked solution would affect the series of interferent-spiked solutions to the same extent, and this can be compensated for by taking

blank readings of a solution containing the interferent salt only. Readings were made in triplicate and corrected for the blank readings as shown in Tables 3-9. The ratios E'/E were calculated and plotted as a function of the analyte concentration in test solution in Figs 3 and 4 for the ICP and flame experiments, respectively.

Table 3. E'/E values: Effect of excess Li interferent on Ca II * (λ = 393.6 nm)

[Ca] mg/L	E [Li]= 0 mg/L	E' [Li] = 1000 mg/L	E'/E (Exp)
0.2	778553±6645	2081694±1484	2.67
0.4	1235614±1237	2689027±6978	2.18
0.6	1908893±2111	3626017±1882	1.90
0.8	2721784±4162	4079534±2820	1.50
2.0	8306215±7933	8355747±1425	1.01
4.0	14615291±5822	14617597±579	1.00
8.0	32097324±1829	29707464±2815	0.93
10.0	33203770±1859	33214872±4407	1.00
14.0	53349413±1126	49002586±2537	0.92
20.0	78537595±1057	67945785±5195	0.87
30.0	115421032±1566	99705488±3163	0.83

^{*}M I refers to emission from M atomic line, whereas M II refers to emission from M ionic line.

Table 4. E'/E values: Effect of excess K interferent on Sr II (λ = 407.8 nm)

[Sr] mg/L	E [K]= 0 mg/L	E' [K] = 1000 mg/L	E'/E (Exp)
0.1	846 <u>+</u> 9	1968 <u>+</u> 25	2.33
0.2	1114 <u>+</u> 12	2425 <u>+</u> 16	2.18
0.4	2410 <u>+</u> 26	3262 <u>+</u> 57	1.35
0.6	3384 <u>+</u> 35	4380 <u>+</u> 74	1.29
8.0	5492 <u>+</u> 64	6683 <u>+</u> 34	1.22
1.0	10225 <u>+</u> 201	11958 <u>+</u> 123	1.17
2.0	13138 <u>+</u> 319	14427 <u>+</u> 241	1.10
4.0	18768 <u>+</u> 213	20070 <u>+</u> 127	1.07
8.0	24390 <u>+</u> 412	25786 <u>+</u> 312	1.06
12.0	31603 <u>+</u> 129	32896 <u>+</u> 213	1.04
16.0	47046 <u>+</u> 712	48556 <u>+</u> 265	1.03
20.0	84625 <u>+</u> 345	87443 <u>+</u> 512	1.03
30.0	117868 <u>+</u> 617	122300 <u>+</u> 819	1.04

Table 5. E'/E values: Effect of excess Li interferent on Sr II (λ = 407.8 nm).

[Sr] mg/L	E [Li]= 0 mg/L	E' [Li] = 1000 mg/L	E'/E (Exp)
0.4	077.44	4000 : 40	0.00
0.1	877 <u>+</u> 11	1983 <u>+</u> 13	2.26
0.2	1178 <u>+</u> 10	2179 <u>+</u> 9	1.85
0.4	2182 <u>+</u> 33	3033 <u>+</u> 35	1.39
0.6	3590 <u>+</u> 58	4488 <u>+</u> 52	1.25
8.0	5651 <u>+</u> 46	6679 <u>+</u> 43	1.18
1.0	9976 <u>+</u> 122	11482 <u>+</u> 119	1.15
2.0	13388 <u>+</u> 253	14606 <u>+</u> 250	1.09
4.0	20044 <u>+</u> 232	20986 <u>+</u> 256	1.05
8.0	26421 <u>+</u> 324	27399 <u>+</u> 336	1.04
12.0	34207 <u>+</u> 315	34789 <u>+</u> 345	1.02
16.0	37960 <u>+</u> 467	38909 <u>+</u> 412	1.03
20.0	41483 <u>+</u> 513	42271 <u>+</u> 522	1.02
30.0	47523 <u>+</u> 815	49376 <u>+</u> 789	1.04

Table 6. E'/E values: Effect of excess K interferent on Mg II (λ = 279.6 nm).

[Mg] mg/L	E [K]= 0 mg/L	E' [K] = 1000 mg/L	E'/E (Exp)
0.1	757 <u>+</u> 8	1994 <u>+</u> 21	2.64
0.2	4412 <u>+</u> 12	7600 <u>+</u> 23	1.72
0.4	9112 <u>+</u> 35	12469 <u>+</u> 46	1.37
8.0	26990 <u>+</u> 43	30632 <u>+</u> 35	1.14
1.0	37674 <u>+</u> 123	41769 <u>+</u> 121	1.11
2.0	47165 <u>+</u> 245	50872 <u>+</u> 243	1.08
4.0	99252 <u>+</u> 149	104661 <u>+</u> 132	1.06
8.0	196602 <u>+</u> 324	210246 <u>+</u> 320	1.07
12.0	283660 <u>+</u> 333	296878 <u>+</u> 217	1.05
16.0	365027 <u>+</u> 349	383570 <u>+</u> 267	1.05
20.0	401268 <u>+</u> 436	426789 <u>+</u> 456	1.06
30.0	518270 <u>+</u> 784	532781 <u>+</u> 728	1.03

Table 7. E'/E values: Effect of excess Li interferent on Mg II (λ = 279.6 nm)

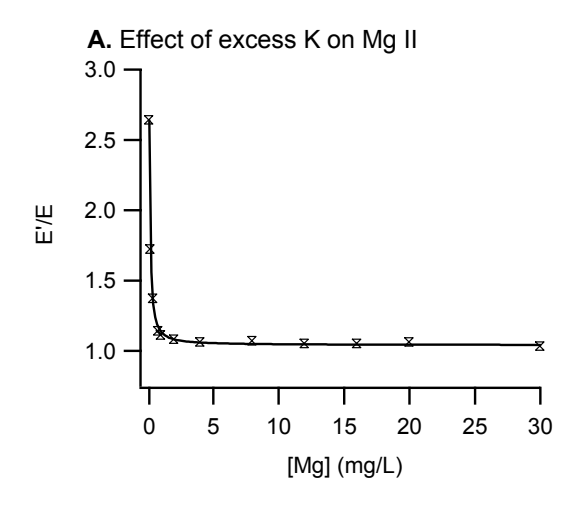
[Mg]	E	E'	E'/E
mg/L	[Li]= 0 mg/L	[Li] = 1000 mg/L	(Exp)
0.1	1346 <u>+</u> 23	3273 <u>+</u> 36	2.43
0.2	7552 <u>+</u> 45	12294 <u>+</u> 41	1.63
0.4	15808 <u>+</u> 78	22150 <u>+</u> 62	1.40
0.6	32533 <u>+</u> 76	40521 <u>+</u> 77	1.25
8.0	53742 <u>+</u> 78	61776 <u>+</u> 67	1.15
1.0	73857 <u>+</u> 130	83303 <u>+</u> 121	1.13
2.0	91115 <u>+</u> 245	100318 <u>+</u> 253	1.10
4.0	176564 <u>+</u> 197	191024 <u>+</u> 189	1.08
12.0	779988 <u>+</u> 1578	823121 <u>+</u> 1778	1.06
16.0	1373761 <u>+</u> 1623	1445334 <u>+</u> 1567	1.05
20.0	1695955 <u>+</u> 1216	1726821 <u>+</u> 1187	1.02
30.0	2268479 <u>+</u> 1498	2300465 <u>+</u> 1589	1.01

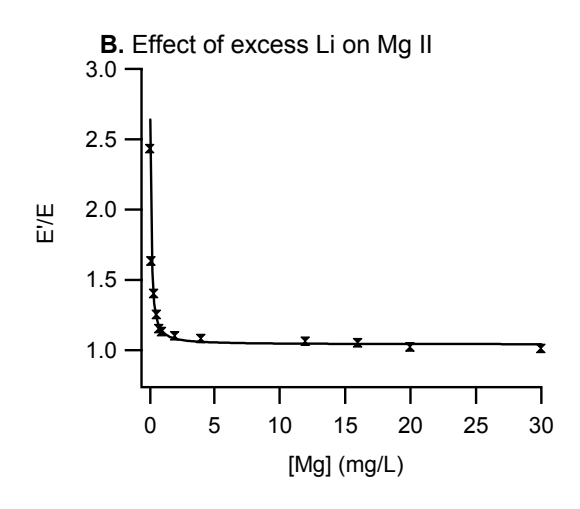
Table 8. E'/E values: Effect of excess Na interferent on K I (λ = 766.5 nm)

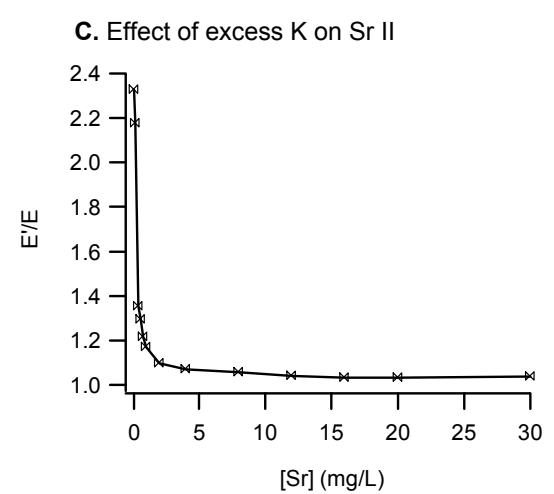
[K] mg/L	E [Na]= 0 mg/L	E' [Na] = 1000 mg/L	E'/E (Exp)
0.25	1196 <u>+</u> 43	2954 <u>+</u> 10	2.47
0.45	3293 <u>+</u> 52	7600 <u>+</u> 11	2.31
0.65	5195 <u>+</u> 47	12469 <u>+</u> 25	2.40
0.85	10793 <u>+</u> 35	21229 <u>+</u> 32	1.97
1.05	17257 <u>+</u> 122	30632 <u>+</u> 199	1.78
2.05	28550 <u>+</u> 235	41769 <u>+</u> 289	1.46
4.05	37303 <u>+</u> 128	50583 <u>+</u> 312	1.36
6.05	92375 <u>+</u> 315	104661 <u>+</u> 401	1.13
8.05	176529 <u>+</u> 237	210246 <u>+</u> 452	1.19
10.05	254646 <u>+</u> 298	287750 <u>+</u> 369	1.13
14.05	335312 <u>+</u> 312	361802 <u>+</u> 617	1.08
20.05	422314 <u>+</u> 501	451876 <u>+</u> 567	1.07
30.05	523663 <u>+</u> 829	561890 <u>+</u> 710	1.07

Table 9. E'/E values: Effect of excess K interferent on Mg I (λ = 285.2 nm), Flame Experiment . (n = 5)

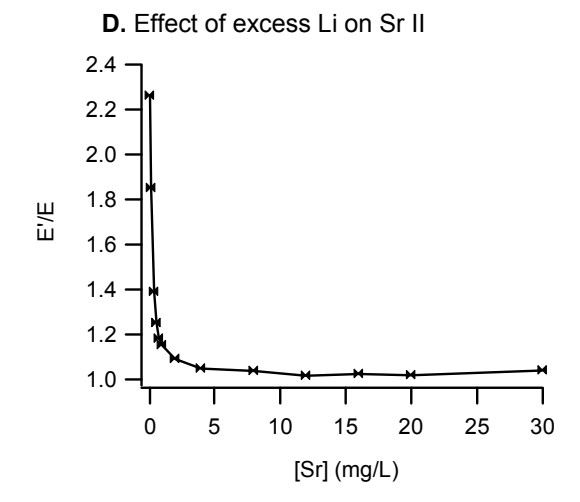
[Mg] mg/L	E [K]= 0 mg/L	E' [K] = 1000 mg/L	E'/E (Exp)
0.1	0.0004±0.0001	0.0007±0.0006	1.75
0.2	0.0016 <u>+</u> 0.0002	0.0026 <u>+</u> 0.0003	1.64
0.4	0.0032 <u>+</u> 0.0007	0.0048 <u>+</u> 0.0005	1.48
0.6	0.0043 <u>+</u> 0.0010	0.0059 <u>+</u> 0.0009	1.37
0.8	0.0071 <u>+</u> 0.0009	0.0087 <u>+</u> 0.0006	1.23
1.0	0.0152 <u>+</u> 0.0013	0.0182 <u>+</u> 0.0012	1.20
2.0	0.0297 <u>+</u> 0.0023	0.0351 <u>+</u> 0.0016	1.18
4.0	0.0563 <u>+</u> 0.0078	0.0674 <u>+</u> 0.0059	1.20
8.0	0.1001 <u>+</u> 0.0098	0.1175 <u>+</u> 0.0101	1.17
12.0	0.1797 <u>+</u> 0.0100	0.1971 <u>+</u> 0.0099	1.10
16.0	0.2211 <u>+</u> 0.0078	0.2355 <u>+</u> 0.0102	1.07
20.0	0.2396 <u>+</u> 0.0099	0.2569 <u>+</u> 0.0074	1.07
30.0	0.4285 <u>+</u> 0.0110	0.4589 <u>+</u> 0.0123	1.07







E. Effect of excess Li on Ca II



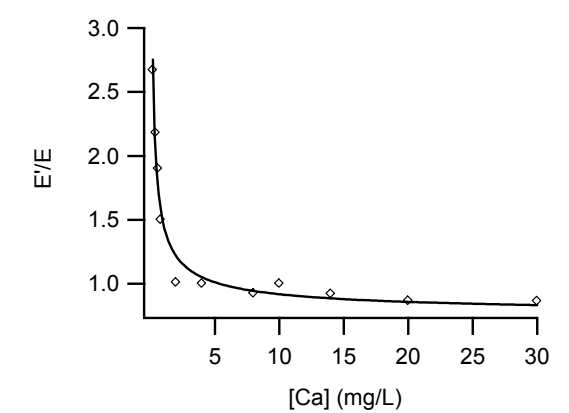
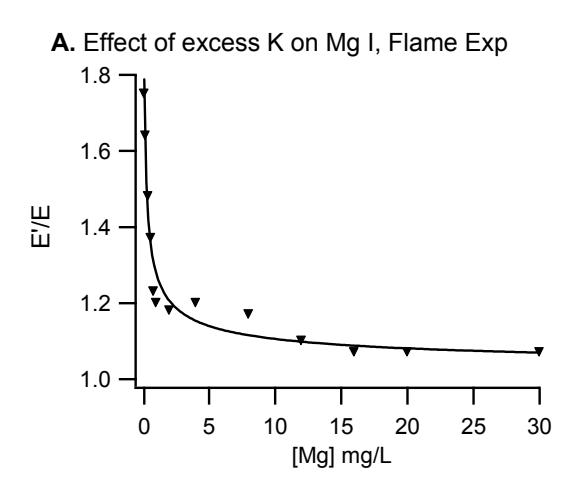


Fig. 3. Experimental E'/E for Ca II, Mg II, and Sr II ICP-AES lines Vs Ca, Mg, and Sr concentration in test solution for the effect of Li and K.



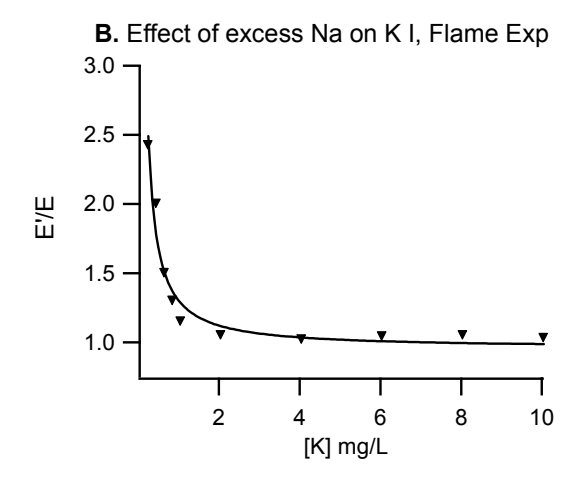


Fig. 4. Effect of 1000 mg/L Na on K atom line (A) and of 1000 mg/L K on Mg atom line (B) in the air-acetylene flame.

2.3.5 Average Aspiration Rate Determination

In the determination of the average aspiration rate, the following solutions were used: 30 ppm Mg; 10 ppm Mg in the presence of 1000 ppm Li and deionised water. For each type of solution, twenty replicates were run. Practically, this was done by determining the time a given volume of solution, of a given mass is aspirated. The individual aspiration rates were calculated for the twenty replicates as per solution composition. The data were treated statistically using the Q-test for the rejection of values well outside the normal distribution at 90% confidence interval level. An average aspiration rate for each solution was calculated and the standard deviations determined.

Based on the individual average aspiration rates for the different solutions, the overall average aspiration rate was also determined based on the individual solution type. Table 10 below shows a summary of the determinations;

Table 10. Experimental determination of aspiration rate, ICP experiments*.

Solution Investigated ppm	Average Flow Rates	Averaged Flow Rate at 99% Confidence Level g min ⁻¹
30 Mg	1.00 <u>+</u> 0.01	1.00 <u>+</u> 0.01
10 Mg + 1000 Li	1.03 <u>+</u> 0.02	1.03 <u>+</u> 0.02
1000 Li	0.98 <u>+</u> 0.05	0.98 <u>+</u> 0.05
Deionised water	1.00 <u>+</u> 0.02	1.00 <u>+</u> 0.02
Average	1.00 <u>+</u> 0.04	1.00 <u>+</u> 0.01

 $^{^*}h = 8$ and n = 5, where h = number of samples and <math>n = number of replicates.

The average aspiration rate was done for both volume of solution aspirated and mass of solution aspirated. The liquid must pass on to the atomizer at a uniform rate. The quantity aspirated per unit time should be, as nearly as possible, constant for a given solution type. Be it so changes in the properties of the solution (surface tension, density, viscosity, etc) can affect aspiration rate, hence it is important to establish the aspiration rate.

Results in Table (10) above indicate that, for the solutions used, the change in ionic concentration did not cause a significant variation in the aspiration rate. Aspiration rates for both mass and volume of solution had a negligible difference.

Average aspiration rate: 1.00±0.04 g min⁻¹

2.3.6 Nebulization Efficiency Determination

The efficiency of nebulization (spraying) controls the fraction of sample solution converted into tiny droplets (liquid aerosol) which can ultimately reach the flame. It is governed by such parameters as the viscosity and surface tension of the sample solution, the flow rate of the nebulizer gas, and the design of the nebulizer itself.

In the determination of nebulization efficiency, solutions of differing ionic strengths were used. Solutions containing high solute concentrations have relatively high viscosities — which cause a decrease in the amount of sample nebulized and a consequent reduction in the number of free atomic vapour in the flame/plasma. Nebulization efficiency was determined by finding the mass of solution aspirated and then collecting the solution released at the drain pipe (residual solution). The mass or volume of solution nebulized was the difference between the total mass/volume aspirated and mass/volume of residual solution collected at the drain. This was done for n = 5. Data collected were subjected to the Rejection Test at 90% confidence levels.

Table (11) below shows the results of experimental determination of the nebulization efficiency.

Table 11. Experimental determination of nebulization efficiency, ICP experiments.

Initial mass of Solution /g	Mass of solution recovered /g	Mass of solution nebulized /g	Nebulization efficiency %
9.8792	9.3068	0.5724	5.79
8.6987	8.2035	0.4952	5.69
10.5676	9.9812	0.5864	5.55
9.2167	8.7213	0.4954	5.38
9.9346	9.3867	0.5479	5.52
9.8989	9.2346	0.6643	6.71
9.8946	9.3269	0.5677	5.74
9.9335	9.3678	0.5657	5.69

 $^{^*}h = 12 \text{ and } n = 5$

Average nebulization efficiency = 5.75±0.41 %.

The aspiration rate and nebulization efficiency for Flame experiments were obtained in the same way and found to be 4.0 ± 0.1 g/min (h = 8 and n = 5) and $5.44\pm0.20\%$ respectively.

2.4.0 Results and discussion

Figure 3 shows the experimental E'/E curves for the effect of excess Li on Ca atom line and excess Li and K on the Ca, Mg and Sr ion lines. Figure 4 shows the experimental E'/E curves for the effects of Na on K and K on Mg line mission in the air-acetylene flame. The curves in both figures show a sharp increase in line emission signal enhancement with decrease in the concentration of the analyte in the test solution below about 0.5 mg/L. The similarity between the curves for the ICP and flame experiments suggests (a) that the effects of EIE's are due entirely to the presence of the interferent, i.e., the differences in the temperature and composition of the ICAP and that of the air-acetylene are not significant as far as emission signal enhancement is concerned, (b) argon species do not contribute significantly to the analyte emission signal enhancement in ICP, and (c) the effects of EIEs in flame AES and ICP AES can be represented by the same kinetic model.

As pointed out above, collisional excitation can result from electronic collisions (electron impact excitation or ion-electron radiative recombination), or charge transfer involving analyte ions and activated interferent atoms. The apparent non-involvement of electrons from the ionization of Ar can be a statistical effect as proposed by Zaranyika and Chirenje. Other possible reasons are (a) ambipolar diffusion, (b) dominance of charge transfer involving analyte ions and activated interferent atoms.

Ambipolar diffusion was discussed in the Introduction Section. In a gas containing an appreciable quantity of ions and electrons, because of their small mass, electrons tend to diffuse faster than ions. The resultant charge separation produces an electric field which retards the diffusion velocity of electrons, and increases that of ions, until a state of balance is reached in which ions and electrons

diffuse with the same velocity. In this state, the ion and electron behave as an ion pair, and the electron is not completely free and therefore not capable of random motion. In fact equilibrium is to be expected between electron in the ambipolar diffusion layer and free electrons in the continuum or Maxwellian region. The number density of electrons in the ambipolar diffusion layer will depend on the ionization potential of the atom and temperature of the plasma. The net result of ambipolar diffusion is to reduce the number density of free electrons. Ambipolar diffusion is common in plasmas [19, 47, 65, 69-72]. The apparent unavailability of electrons from the ionization of Ar for collisional excitation suggests that ambipolar diffusion reduces the number density of electrons from the ionization of Ar to below those of the analyte.

Charge transfer involving analyte ion and interferent activated atoms was described previously by Zaranyika, Nyakonda and Moses [100] for collisional charge transfer between K⁺ ions and activated Na atoms. Unlike electronic collisions where the activation energy must at least be equal to the ionization potential of the analyte plus its excitation energy (for radiative recombination), the activation energy in activated charge transfer, equal to the difference between analyte excited state and interferent ground state, is less than analyte ionization potential when the interferent is an EIE.

CHAPTER 3

PROPOSED SIMPLIFIED RATE MODEL BASED ON CHARGE TRANSFER TO ACCOUNT FOR THE NON-INVOLVEMENT OF ELECTRONS FROM THE IONIZATION OF ARGON IN INTERFERENCE EFFECTS DURING ICP-OES.

3.1 Theoretical

The mechanism of collisional charge transfer between analyte and interferent was discussed previously [140-146]. A possible mechanism for the collisional charge transfer between Li atoms and Ca⁺ ions is shown in Fig. 5. In actual practice, charge transfer can be envisaged to proceed with activation of the Li atoms prior to collision.

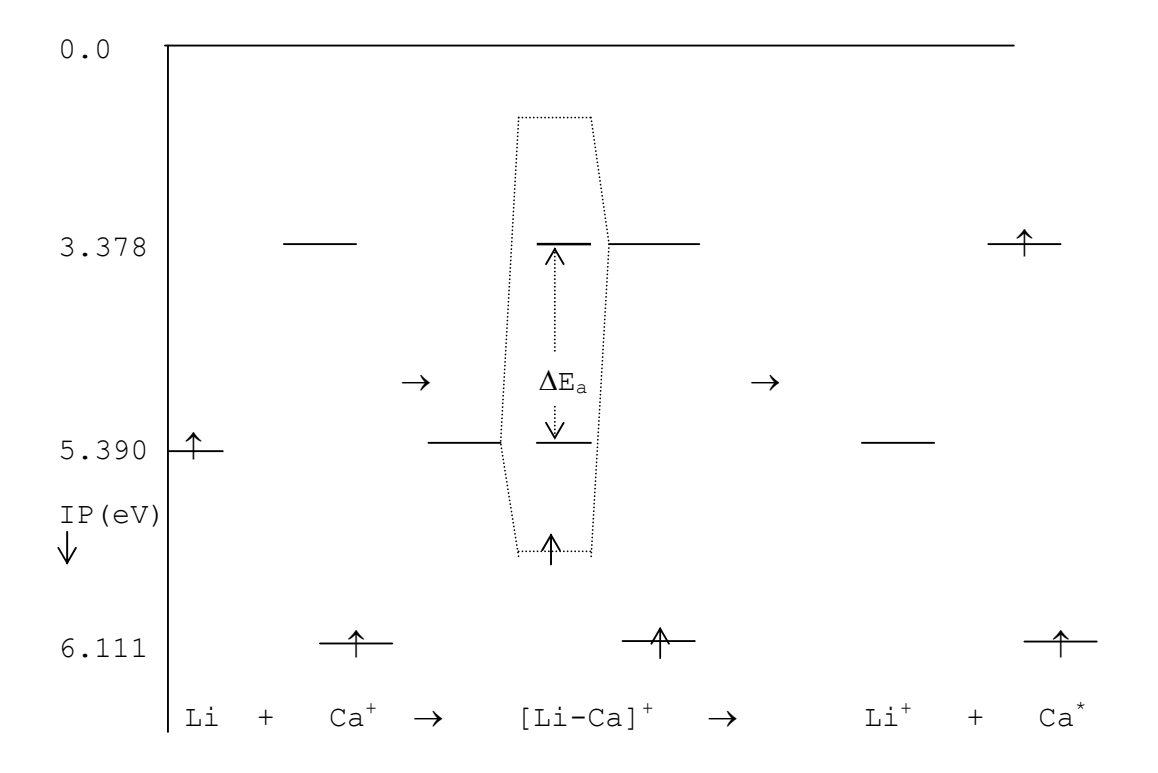


Fig. 5. Possible mechanism of collisional charge transfer between the Li atom and Ca⁺ ion to give Ca⁺ excited state.

In the ICP, $n_{(Ar+)} >> n_{(A+)} + n_{(m+)}$, which suggests that the ICP plasma is dominated by electrons from the ionization of Ar. The non-involvement of Ar in the signal enhancement means that electronic collisions cannot be the major source of the signal enhancement. Charge transfer between analyte and interferent species may occur to yield excited atoms or ions. A possible simplified rate model is shown in Fig. 6 below.

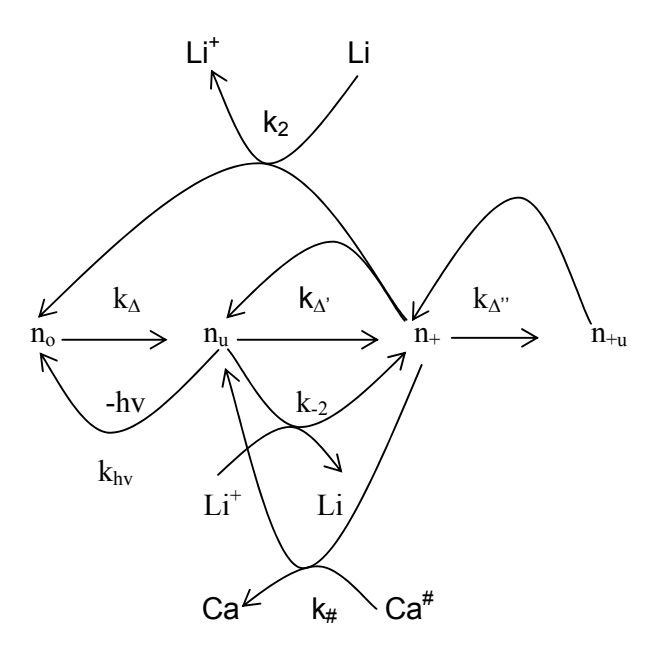


Fig. 6. Schematic diagram of the model incorporating charge transfer process. # denotes all species derived from analyte (M) other than M²⁺ ions

Assuming a steady state with respect to analyte excited state, we have:

$$d[Ca^{\dagger}]/dt = 0 = k_A[Ca] + k_H[Ca^{\dagger}][Ca^{\dagger}] + k_2[Li][Ca^{\dagger}] - k_2[Ca^{\dagger}][Li^{\dagger}] - k_{bv}[Ca^{\dagger}]$$

Therefore

$$[Ca^*]' = \frac{k_{\Delta}[Ca] + k_{\#}[Ca^+][Ca^\#] + k_{2}[Li][Ca^+]}{k_{hv} + k_{-2}[Li^+]}$$
(71)

where the prime denotes presence of interferent. In the absence of interferent

$$[Ca*] = \frac{k_{\Delta}[Ca] + k_{\#}[Ca^{+}][Ca^{\#}]}{k_{bv}}$$
(72)

Dividing eq. 71 by 72

$$\frac{[Ca^*]'}{[Ca^*]} = \left\{ 1 + \frac{k_2[Li][Ca^+]}{k_{\Delta}[Ca] + k_{\#}[Ca^+][Ca^\#]} \right\} \left\{ \frac{k_{hv}}{k_{hv} + k_{-2}[Li^+]} \right\}$$
(73)

The rate of collisional charge transfer is derived from collision theory, and is given by

$$k_2[Li][Ca^+] = k_c[Li][Ca^+].\exp(-\Delta E_a/kT)$$
 (74)

where the collisional rate constant, $k_C = \pi d_{12}^2 (8kT/\pi\mu)^{1/2}$ [152], ΔE_a is the activation energy, d_{12} is the mean diameter of the colliding species, and μ is the reduced mass.

The rates calculated for the various processes are shown in Tables 12 and 13.

Table 12. Rates calculated for processes in eq. 72.

Process	Rate equation for Cal/Li*	Rate of process (s ⁻¹)
k∆[Ca]	[Ca]g _u /g _o .exp(-2.933 eV/kT)	8.4479 x 10 ⁸ c
k₂[Li][Ca ⁺]	k _c [Li][Ca ⁺].exp(-2.022 eV/kT)	3.6178 x 10 ¹⁴ c
k _# [Ca ⁺][Ca [#]]	α (1- α) k _c [Ca] ²	1.3799 x 10 ¹⁰ c ²
k₋₂[Ca [*]][Li ⁺]	$k_c[Li^{\dagger}][Ca]g_u/g_o.exp(-2.933/kT)$	5.1571 x 10 ¹⁴ c
$k_{hv}n_u$	K _{hv} [Ca]g _u /g _o .exp(-2.933 eV/kT)	3.1521 x 10 ¹⁷ c

^{*}Analyte/Interferent; α = degree of ionization.

Table 13. Rates of limiting steps for processes in eq. 73.

Process	Rate of Cal/Li* system	Rate/values for limiting step
k _∆ [Ca]	k₄[Ca] s⁻¹	8.4479 x 10 ⁸ c
k₂[Li][Ca ⁺]	$n_{(Li)} s^{-1}$	1.4367 x 10 ¹⁴
k _# [Ca ⁺][Ca [#]]	$[Ca^{\#}] = (1-\alpha)N_{(Ca)} s^{-1}$	2.7361 x 10 ⁸ c
k₋₂[Ca [*]][Li ⁺]	$n_{(Li+)} s^{-1}$	1.4367 x 10 ¹⁴
$k_{hv}n_u$	K_hv	3.7312 x 10 ⁸

^{*}Analyte/Interferent; α = degree of ionization.

Taking these rates (in Table 13) into account, eq. 73 can be generalized to

$$\frac{n_{u}'}{n_{u}} = \left[1 + \frac{n_{(m)}}{k_{\Delta}n_{(a)} + (1 - \alpha)n_{(a)}}\right] \left[\frac{k_{hv}}{k_{hv} + n_{(m^{+})}}\right]$$
(75)

By assuming $(n_{(a)}/k_{\Delta}n_{(a)}) >> 1$ and making appropriate substitution, it can be shown that eq. 75 converts to eq. 76, thus:

$$\frac{n_{u}'}{n_{u}} = 1 + \left[\frac{n_{(m)}}{k_{\Delta} n_{(a)} + (1 - \alpha) n_{(a)}} \right] \left[\frac{k_{hv}}{k_{hv} + n_{(m^{+})}} \right]$$
(76)

After substituting the appropriate values from Tables 12 and 13, we arrive at eq. 77 for the effects of 1000 mg/L Li on the Ca atom line:

$$(n_u'/n_u)_{Cal/Li} = 1 + 4.4405 \times 10^{-1}/c$$
 (77)

where c is analyte concentration.

For the Ca ion line, assuming $[Ca^{\#}] >> [Ca^{2+}]$, where $Ca^{\#}$ represents all species derived from Ca, other than Ca^{2+} ions gives;

$$\frac{n_u'}{n_u} = 1 + \left[\frac{n_{(m)}}{k_{\Delta} n_{(a)} + n_{(a^{2+})}} \right] \left[\frac{k_{hv}}{k_{hv} + n_{(m^+)}} \right]$$
 (78)

where $n_{a^{2+}} = [Ca^{2+}]$

For the effects of 1000 mg/L Li or K on Ca, Mg and Sr ion lines:

$$(n_u'/n_u)_{Call/M} = 1 + 2.7246 \times 10^{-1}/c$$
 (79)

$$(n_u'/n_u)_{MgII/M} = 1 + 3.1564 \times 10^{-1}/c$$
 (80)

$$(n_u'/n_u)_{SrII/M} = 1 + 1.4968 \times 10^{-1}/c$$
 (81)

where the subscript M denotes interferent element, in this case Li or K.

For systems in the air-acetylene flame, [Ca[#]] >> [Ca⁺] because of the low degree of ionization of the analyte at the low flame temperature. In addition analytes are only ionized to a very low extent in the air-acetylene. Easily ionized elements enhance analyte ionization, as well as excitation, through charge transfer as follows:

(i)
$$K^+ + Mg \rightarrow Mg^+ + K$$

(ii)
$$K + Mg^{+} \rightarrow Mg^{*} + K^{+}$$

The rate-determining step is (i), hence eq. 78 becomes

$$\frac{n_{u}'}{n_{u}} = 1 + \left\lceil \frac{n_{(m^{+})}}{k_{\Delta}n_{(a)} + n_{(a^{+})}} \right\rceil \left\lceil \frac{k_{hv}}{k_{hv} + n_{(m^{+})}} \right\rceil$$
(82)

After substituting for k_{Δ} , $k_{h\nu}$, n_{a^+} , n_{m^+} , n_a into eq. 82, we arrive at eqs. 83 and 84 for the effects of 1000 mg/L Na on the K atom line, and 1000 mg/L K on Mg atom line in the air-acetylene flame:

$$(n_u'/n_u)_{K/Na} = 1 + 5.793 \times 10^{-2}/c$$
 (83)

$$(n_u'/n_u)_{Mgl/K} = 1 + 6.8139 \times 10^{-1}/c$$
 (84)

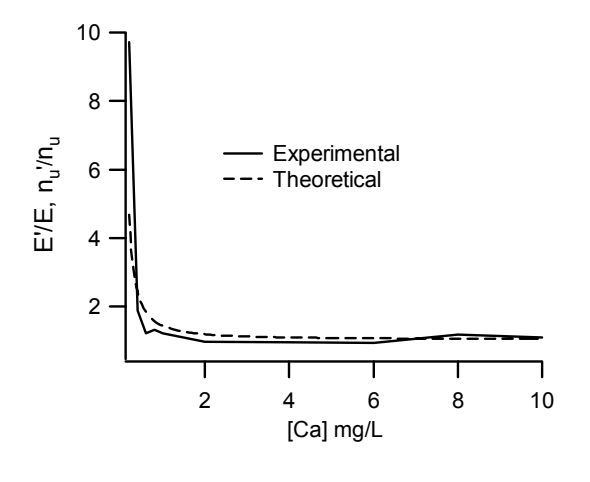
If we assume $E'/E = n_u'/n_u$, then the calibration curve in the presence of excess easily ionized element can be predicted from the appropriate n_u'/n_u equation and line emission readings in the presence of the interferent, according to eq. 85:

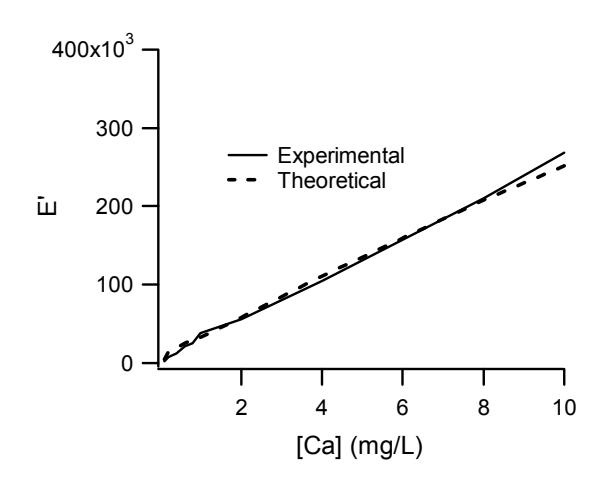
$$E' = E(n_u'/n_u) \tag{85}$$

3.2 Results and Discussion

Fig. 7 shows the n_u'/n_u , experimental and predicted calibration curves for the Ca atom and ion lines in the presence of 1000 mg/L Li as interferent in the ICP. It is apparent from Fig. 7 that reasonable agreement between theory and experiment is obtained. Fig. 8 shows the n_u'/n_u curves and predicted calibration curves for the Mg and Sr ion lines in the presence of 1000 mg/L Li as interferent, while Fig. 9 shows the n_u'/n_u curves and predicted calibration curves for the Mg and Sr ion lines in the presence of 1000 mg/L K as interferent in the ICP. The experimental curves are included for comparison. It is apparent from Figs. 8 and 9 that reasonably good agreement between theory and experiment is obtained ($R^2 = 0.99789$). The somewhat deviations from straight line obtained for all calibration curves could be explained by the possibility of contamination of the interferent salts and experimental errors. For example, a typical AR grade LiCl salt (which contains about 0.005% Ca) in 1000 mg/L Li solution gives 0.05 mg/L Ca contamination. However, the general shapes of the theoretical and experimental curves remain similar in all experiments.

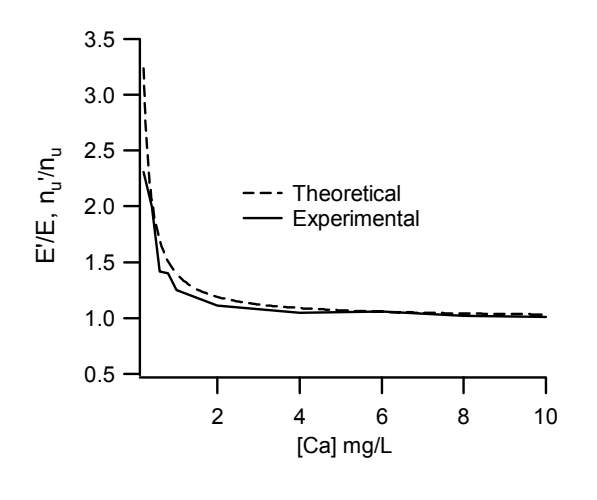
Fig. 10 shows the n_u'/n_u curves and predicted calibration curves for the Mg atom line in the presence of 1000 mg/L K as interferent and the predicted calibration curves for the K atom line in the presence of 1000 mg/L Na as interferent, in the air-acetylene flame. Again the experimental curves are included for comparison. It is apparent from Fig. 10 that good agreement between theory and experiment was obtained for the Charge transfer model.





C. Effect of excess Li on Enhancement Factor for Call





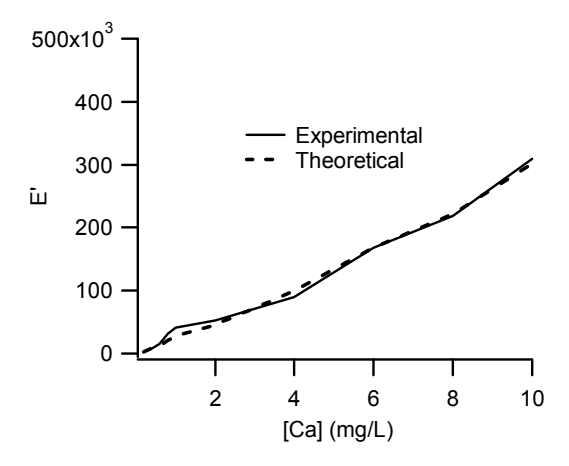
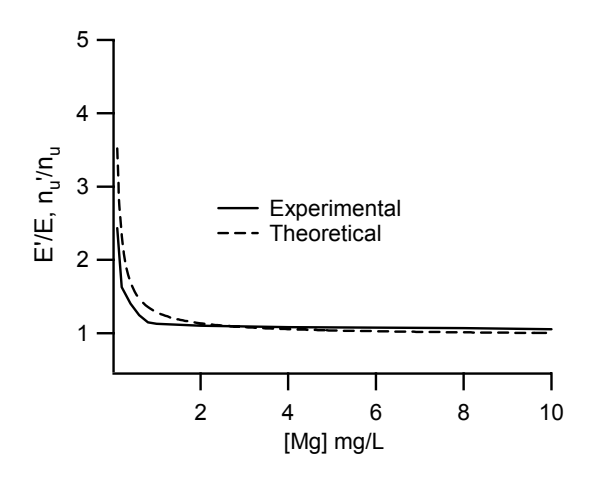
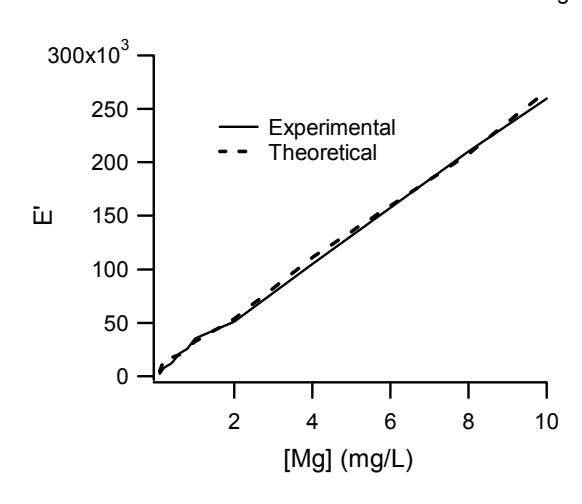


Fig. 7: Effect of 1000 mg/L Li on Ca atom and ion line emission intensity. (*A and B*: Data extracted from Zaranyika and Chirenje [126]; *C and D*: Data is shown in Table 3. Data points were limited to 10 mg/L [Ca] in order to illustrate more clearly the region where change is occurring).

A. Effect of excess Li on Enhancement Factor for MgII

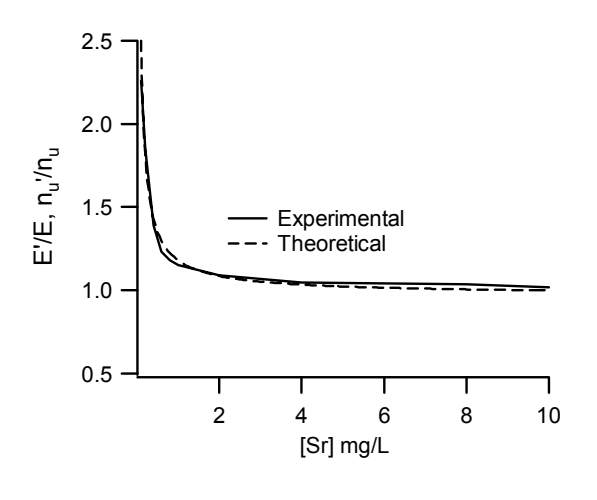






C. Effect of excess Li on Enhancement Factor for SrII

D. Effect of excess Li on Calibration curve for SrII



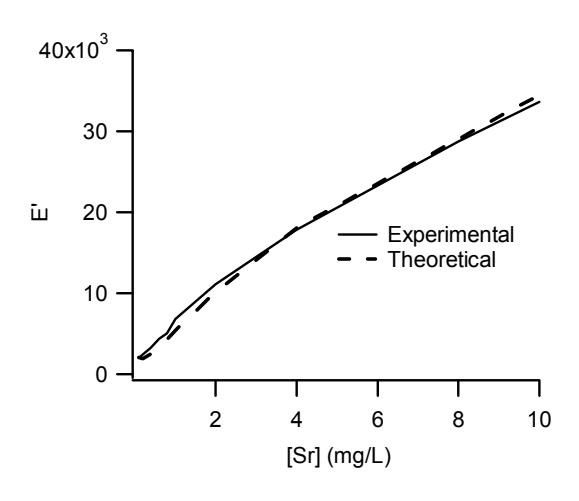
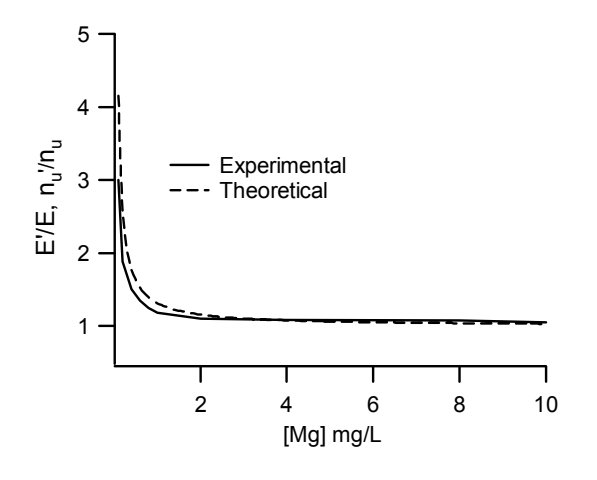
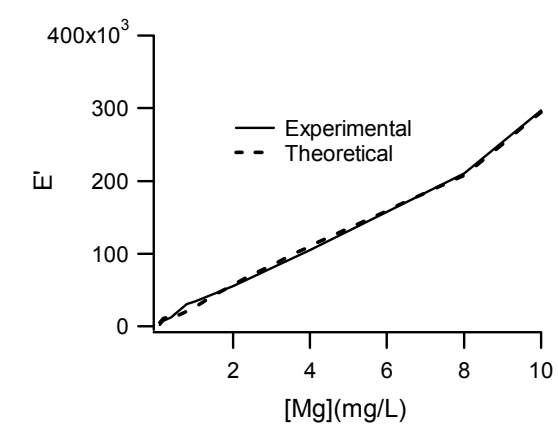


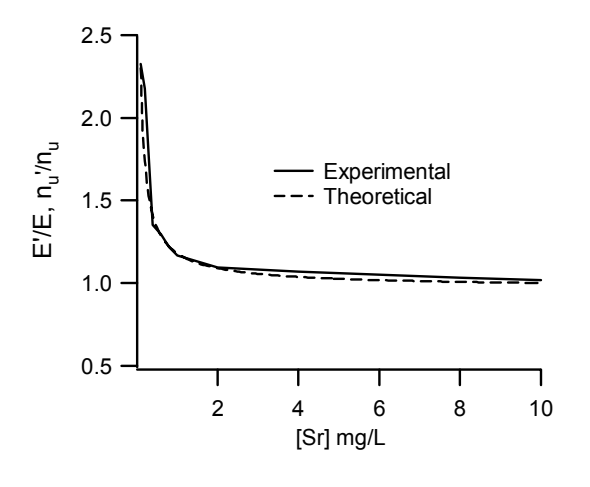
Fig. 8. Effect of 1000 mg/L Li on Mg and Sr ion line emission intensity and calibration curves in the ICP. (Data for the plots are shown in Tables 5 and 7. Data points were limited to 10 mg/L [Ca] in order to illustrate more clearly the region where change is occurring).





C. Effect of excess K on Enhancement Factor for SrII

D. Effect of excess K on Calibration curve for SrII



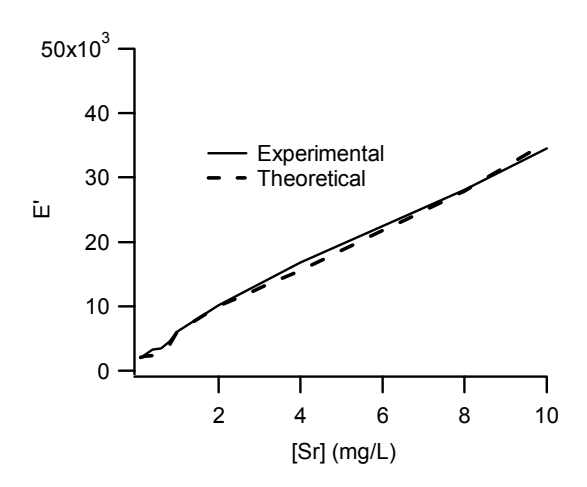
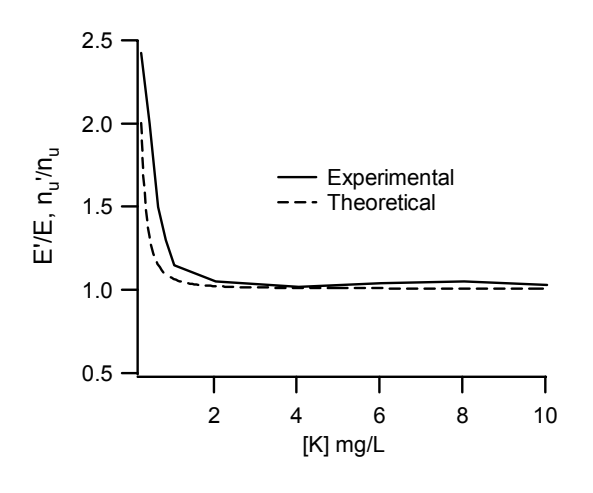
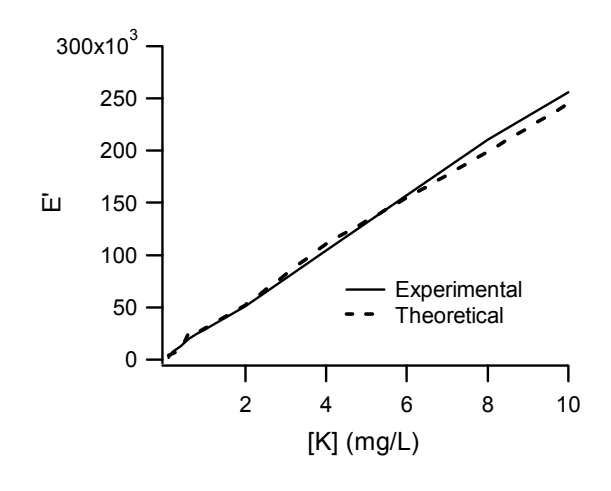


Fig. 9. Effect of 1000 mg/L K on Mg and Sr ion line emission intensity and calibration curves in the ICP. (Data for the plots are shown in Tables 4 and 6. Data points were limited to 10 mg/L [Ca] in order to illustrate more clearly the region where change is occurring).

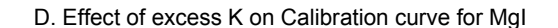
A. Effect of excess Na on Enhancement Factor for K

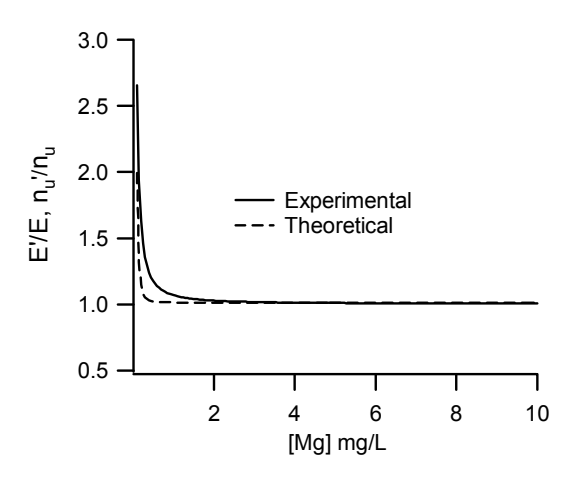






C. Effect of excess K on Enhancement Factor for MgI





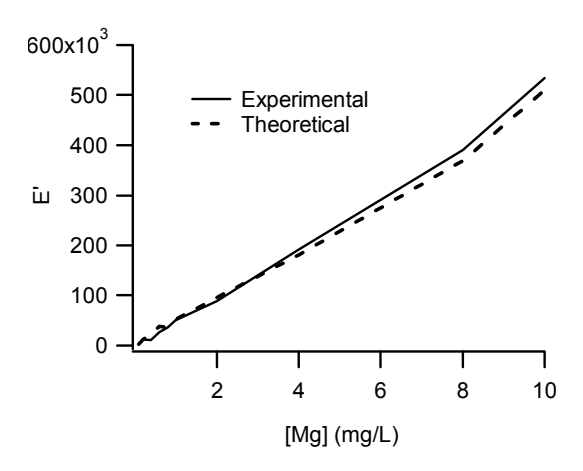


Fig. 10. Effect of 1000 mg/L Na on K line emission, and 1000 mg/L K on MgI line emission in the air-acetylene flame. (Data for the plots are shown in Tables 8 and 9. Data points were limited to 10 mg/L [Ca] in order to illustrate more clearly the region where change is occurring).

The possibility of charge transfer processes contributing to excitation mechanisms in the ICP was discussed by several workers, as described in preceding sections. Penning ionization involving Ar metastable states has been suggested as one process whereby analyte atoms might be ionized or excited [118, 119, 122, 147], the other being charge transfer involving Argon ions [140-146]. The similarity between the E'/E curves for the flame and ICP experiments reported in this work would tend to suggest that the effect of charge transfer processes involving Ar species on analyte excitation is negligible under the experimental conditions employed for the ICP.

Examination of eq. 82 shows that when $n_{(m+)} >> k_{hv}$, eq. it reduces to

$$\frac{n_{u}'}{n_{u}} = 1 + \left[\frac{k_{hv}}{k_{\Delta}n_{(a)} + (1 - \alpha)n_{(a)}}\right] \left[\frac{n_{(m)}}{n_{(m^{+})}}\right]$$
(86)

i.e., the observed emission signal enhancement is an inverse function of the degree of ionization of the interferent (given by $(1-\alpha)$). This is in agreement with the finding by Henselman *et al.* [52], following a study of the effect of sample matrix on electron density, electron temperature in the ICP using Thompson and Rayleigh scattering, that in general the order of n_e and T_e enhancement is an inverse function of the ionization potential of the interferent. The degree of ionization is a very sensitive function of temperature, and may explain in part the spatial variation of emission signal enhancement due to easily ionized elements that has been widely reported [55].

Interference effects from easily ionized element matrices in the ICP were reviewed by Blades and Horlick [31]. These workers concluded that the exact

nature of the interference with the analyte emission is complex. Examination of the calibration curves in Figs. 7 to 9 confirms this. For example, although very good agreement is obtained between experiment and theory for the effect of Li or K on Mg and Sr ion lines, the calibration curves obtained in each case for Mg and Sr exhibit differences which point to the existence of analyte specific factors not readily explainable from this limited work. The same applies to the calibration curves for the effect of Li on Ca atom and ion lines (Fig. 7).

If in eqn 86, we further assume that $\alpha \approx 1$, then the equation reduces to:

$$\frac{n_u'}{n_u} = 1 + \left(\frac{n_{(m)}}{k_{\Delta} n_a}\right) \left(\frac{k_{h\nu}}{n_{m(+)}}\right)$$

$$=1+\frac{k_{hv}}{\alpha k_{\Lambda} n_{a}} \tag{87}.$$

where k_{Δ} , the thermal excitation rate constant is given by equation 87. It follows from Eqn. (87) that plotting E'/E vs $1/n_a$ would give a slope of $k_{h\nu}/k_{\Delta}$ and provides a method for measuring k_{Δ} values experimentally.

The major findings in the chapter were that:

- (a). the effects of easily ionized elements during flame AES and ICP-OES can be described using a simplified rate model based on collisional charge transfer between analyte and interferent species.
- (b). it is possible to predict the calibration curve in the presence of easily ionized elements using a simplified charge transfer model.

CHAPTER 4

PROPOSED SIMPLIFIED RATE MODEL BASED ON AMBIPOLAR DIFFUSSION TO ACCOUNT FOR THE NON-INVOLVEMENT OF ELECTRONS FROM THE IONIZATION OF ARGON IN INTERFERENCE EFFECTS DURING ICP-OES.

4.1 Theoretical

The aim of this chapter was to investigate the possible modification of the kinetic model proposed by Zaranyika and Chirenje [126], to take into account ambipolar diffusion, collisional excitation, and collisional de-excitation of the analyte. The kinetic modelling was based on the model proposed by Zaranyika and Chirenje. The new model assumed that equilibrium exists between electrons in the ambipolar diffusion layer and free electrons in the continuum, and that electrons in ambipolar diffusion layer exist as ion-pair complexes.

A possible kinetic scheme incorporating thermal excitation, collisional excitation, ion-electron collisional recombination to excited state and collisional deactivation is shown in Figure 11.

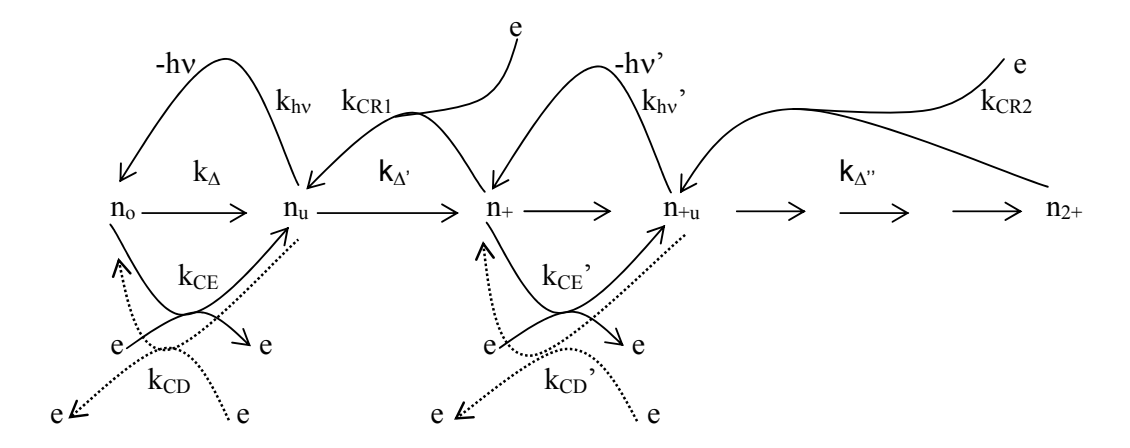


Fig. 11. Schematic representation of the proposed rate model that incorporates ambipolar diffusion (n denotes number density, and the subscripts o, u, and +, denote ground state, excited state, and metal ion respectively; k_{A} = rate constant for thermal excitation from the ground state; $k_{A'}$ = rate constant for thermal excitation from the excited state; k_{CR1} = rate constant for radiative relaxation from the excited state; k_{CR1} = rate constant for ion-electron collisional recombination to the first excited state; k_{CE} = rate constant for collisional excitation).

Assuming a steady state with respect to excited analyte atomic line;

$$\frac{dn_u}{dt} = k_{\Delta} n_o + \alpha k_{CE} n_o n_e + \beta k_{CR(1)} n_+ n_e - k_{hv} n_u - k_{CD} n_u n_e - k_{\Delta}' n_u = 0$$
 (88)

where α , and β denote transition state theory transmission coefficients, n denotes number density, the subscripts o, u, +, e, mo and m+ denote ground state, excited state, ionic state, electron, interferent ground state and interferent ions, respectively; k_{Δ} , k_{CE} , $k_{CR(1)}$, and k_{CD} denote rate constants for thermal excitation, collisional excitation, collisional radiative recombination to give the

excited state, and collisional de-excitation, respectively; α and β denotes the contribution of electron collisional excitation and collisional radiative recombination to the observed line emission signal.

Thermal excitation results from inelastic collisions, other than collisional charge transfer, between the analyte atom or ion with other heavy particles in the plasma. When the cumulative kinetic energy transferred to the analyte atom or ion is equal to the energy required to excite an electron to the next atomic energy level, the energy is converted to internal energy of the atom, resulting in the excitation of the electron. The statistical distribution of atomic species among the various excited states reached via thermal excitation is described by the Boltzman Law of bound states. The Boltzman law, being statistically derived, takes no account of the detailed processes by which equilibrium is reached; hence the statistical distribution of atomic species among the various excited states reached via thermal excitation is a function of temperature only.

In contrast to thermal excitation, collisional excitation and collisional ionization result from collisions with electrons. An electron can excite or ionize an atom provided that its energy is sufficient to provide energy difference between the electronic levels involved. An electron whose kinetic energy is less than the minimum energy required to excite an atom can only make an elastic collision with the atom [86, 87]. Thus electronic collisions lead to specific interactions and the extent of such interactions will depend on the number of electrons undergoing such collisions, and energy of the electrons. The rates for collisional excitation, deexcitation and ionization are therefore derived from collision theory. In radiative recombination, both the kinetic energy and potential energy (of ionization) of the colliding electron have to be converted to radiation [86, 87]. Excitation via

collisional charge transfer involves activated interferent atoms. Collisional deexcitation, i.e., the reverse of excitation by a colliding electron, is a super-elastic collision, in which the excitation energy is given up to the electron as kinetic energy [86, 87].

From eqn 88 three limiting cases can be identified depending on value of α , and β thus:

Limiting Case I (LC I): $\alpha = 0$, $\beta = 0$

$$\frac{dn_{u}}{dt} = k_{\Delta} n_{o} - k_{hv} n_{u} - k_{CD} n_{u} n_{e} - k_{\Delta}' n_{u} = 0$$
(89)

Presence of interferent:

$$n_{u}' = \frac{k_{\Delta} n_{o}}{k_{bu} + k_{\Delta}' + k_{CD}} \tag{90}$$

Absence of interferent:

$$n_u = \frac{k_{\Delta} n_o}{k_{hv} + k_{\Delta}' + k_{CD}}$$

Therefore;

$$\frac{n_u'}{n_u} = 1 \tag{91}$$

i.e., interferents have no effect on thermal excitation. This is consistent with Boltzman Law. Thermal excitation occurs when the random energy of an atom or an electron in a hot gas is sufficient to excite another atom upon collision. The statistical distribution of atomic species among the various excited states reached via thermal excitation is described by the Boltzman Law of bound states. The Boltzman law, being statistically derived, takes no account of the detailed processes by which equilibrium is reached; hence the statistical distribution of atomic species among the various excited states reached via thermal excitation is a function of temperature only. Thus unless the interferent interferes with atomization process or undergoes charge transfer involving analyte excited state, it will not affect the population of the excited state, and hence the emission intensity.

Limiting Case II (LC II): α = 1, β = 0

$$\frac{dn_{u}}{dt} = k_{\Delta} n_{o} + k_{CE} n_{o} n_{e} - k_{hv} n_{u} - k_{CD} n_{u} n_{e} - k_{\Delta}' n_{u} = 0$$
(92)

Assuming $k_{hv} + k_{CD} n_e >> k_{\Delta}$ ', then;

$$\frac{n_{u}'}{n_{u}} = \frac{k_{\Delta} n_{o} + k_{CE} n_{o} n_{e}'}{k_{\Delta} n_{o} + k_{CE} n_{o} n_{e}} \left[\frac{k_{hv} + k_{CD} n_{e}}{k_{hv} + k_{CD} n_{e}'} \right]$$
(93)

$$= \left[1 + \frac{k_{CE}n_{+}n_{m+}}{k_{\Delta}n_{o} + k_{CE}n_{+}}\right] \left[\frac{k_{hv} + k_{CD}n_{+}}{k_{hv} + k_{CD}n_{m+}}\right]$$
(94)

where $n_e = n_+$ and $n_e' = n_{m+}$, provided easily ionized interferents are employed in large excess such that $n_{m+} >> n_+$.

Limiting Case III (LC III): α = 0, β = 1

$$\frac{dn_u}{dt} = k_{\Delta} n_o + k_{CR(1)} n_+ n_e - k_{hv} n_u - k_{CD} n_u n_e - k_{\Delta}' n_u = 0$$
(95)

Assuming $k_{hv} + k_{CD}n_e >> k_{\Delta}$

In the absence of interferent:

$$n_{u} = \frac{k_{\Delta} n_{o} + k_{CR(1)} n_{+} n_{e}}{k_{hv} + k_{CD} n_{e}}$$
(96)

In the presence of interferent:

$$n_{u}' = \frac{k_{\Delta} n_{o} + k_{CR(1)} n_{+} n_{e}'}{k_{hv} + k_{CD} n_{e}'}$$
(97)

Therefore,

$$\frac{n_{u}'}{n_{u}} = \left[1 + \frac{k_{CR(1)}n_{+}n_{e}'}{k_{\Delta}n_{o} + k_{CR(1)}n_{+}n_{e}}\right] \left[\frac{k_{hv} + k_{CD}n_{e}}{k_{hv} + k_{CD}n_{e}'}\right]$$
(98)

$$= \left[1 + \frac{k_{CR(1)}n_{+}n_{m+}}{k_{\Delta}n_{o} + k_{CR(1)}n_{+}^{2}} \left[\frac{k_{hv} + k_{CD}n_{+}}{k_{hv} + k_{CD}n_{m+}} \right]$$
(99)

4.2 Contribution of the individual excitation processes to the observed signal enhancement.

Equations 98 and 99 are composed of an excitation factor (the first factor) and the second factor as the de-excitation factor. Further, eqs 98 and 99 show that the de-excitation factor is composed of similar terms both in the numerator and denominator. Thus any difference in the extent to which one excitation process contributes to the observed signal enhancement, will depend on the excitation factor. The excitation factor on the other hand, is composed of two terms. The first term, 1, defines the situation expected in the absence of interferent, while the second term gives the expected signal enhancement. This term differs in the rate constant used in the two cases.

A further factor that can affect the extent to which a given collisional process contributes to the observed interference effects is the degree of ionization of the analyte. Thermal excitation and collisional excitation involve ground state analyte atoms, whereas collisional radiative recombination involves analyte ions. The relative contribution of thermal excitation and collisional excitation on the one hand, and collisional radiative recombination on the other, will depend on the degree of ionization of analyte atoms. Let the degree of ionization be η , assuming $\alpha = 1$ and $\beta = 1$, then eq. 88 becomes:

$$\frac{dn_{u}}{dt} = (1 - \eta)k_{\Delta}n_{o} + (1 - \eta)k_{CE}n_{o}n_{e} + k_{CR(1)}n_{+}n_{e} - k_{hv}n_{u} - k_{CD}n_{u}n_{e} - k_{CTu}n_{u}n_{m+} - k_{\Delta}'n_{u} = 0$$
(100)

Ambipolar diffusion is the diffusion of charged particles under the influence of an electric field [87, 88, 89, 135]. Electrons in the plasma tend to diffuse faster than ions which is related to their smaller mass. The resultant separation of charge produces an electric field which exerts its force in such a way as to increase the drift velocity of ion species and retard the drift velocity of electrons. Hence ambipolar diffusion is expected to reduce the number of electrons available for the collisional process and for a particle p, a fraction $(1-\chi_p)n_{e(p)}$ will be available for collision, where χ_p represents the fraction associated in ambipolar diffusion ion-pair complex. If we factor in ambipolar diffusion, we have:

$$\frac{dn_{u}}{dt} = (1 - \eta)k_{\Delta}n_{o} + (1 - \eta)k_{CE}n_{o}[(1 - \chi_{a})n_{e(a)} + (1 - \chi_{Ar})n_{e(Ar)}]
+ k_{CR(1)}[(n_{+(a)} + n_{+(Ar)})][(1 - \chi_{a})n_{e(a)} + (1 - \chi_{Ar})n_{e(Ar)}] - k_{hv}n_{u}
- k_{CD}n_{u}[(1 - \chi_{a})n_{e(a)} + (1 - \chi_{Ar})n_{e(Ar)}] - k_{CT}n_{u}[n_{+(a)} + n_{+(Ar)} + n_{+(m)}] - k_{\Delta}'n_{u} = 0$$
(101)

where:
$$n_e = (1 - \chi_a) n_{e(a)} + (1 - \chi_{Ar}) n_{e(Ar)}$$

$$n_e' = (1 - \chi_a) n_{e(a)} + (1 - \chi_{Ar}) n_{e(Ar)} + (1 - \chi_m) n_{e(m)}$$

$$n_+ = n_{+(a)} + n_{+(Ar)}$$

$$n_+' = n_{+(a)} + n_{+(Ar)} + n_{+(m)}$$

and $n_{e(a)}$, $n_{e(Ar)}$, $n_{e(m)}$, $n_{+(a)}$, $n_{+(m)}$, $n_{+(Ar)}$ denotes electron number density due to ionization of analyte, argon and interferent; analyte ion number density, interferent ion number density and argon ion number density respectively.

In the ICP, $\eta \sim 1$, and hence eq 101 reduces to:

$$\frac{dn_{u}}{dt} = k_{CR(1)}[(n_{+(a)} + n_{+(Ar)})][(1 - \chi_{a})n_{e(a)} + (1 - \chi_{Ar})n_{e(Ar)}] - k_{hv}n_{u}
- k_{CD}n_{u}[(1 - \chi_{a})n_{e(a)} + (1 - \chi_{Ar})n_{e(Ar)}] - k_{CT}n_{u}[n_{+(a)} + n_{+(Ar)} + n_{+(m)}] - k_{\Delta}'n_{u} = 0$$
(102)

It follows from eq. 102 that in the absence of interferent:

$$n_{u} = \frac{k_{CR(1)}[(n_{+(a)} + n_{+(Ar)})][(1 - \chi_{a})n_{e(a)} + (1 - \chi_{Ar})n_{e(Ar)}]}{k_{hv} + k_{CD}[(1 - \chi_{a})n_{e(a)} + (1 - \chi_{Ar})n_{e(Ar)}] + k_{CT}[(n_{+(a)} + n_{+(Ar)}] + k_{\Delta}}$$
(103)

and in the presence of interferent:

$$n_{u}' = \frac{k_{CR(1)}[(n_{+(a)} + n_{+(Ar)})][(1 - \chi_{a})n_{e(a)} + (1 - \chi_{Ar})n_{e(Ar)} + (1 - \chi_{m})n_{e(m)}]}{k_{hv} + k_{CD}[(1 - \chi_{a})n_{e(a)} + (1 - \chi_{Ar})n_{e(Ar)} + (1 - \chi_{m})n_{e(m)} + k_{CT}[(n_{+(a)} + n_{+(Ar)} + n_{+(m)}] + k_{\Delta}'}$$
(104)

Therefore, assuming that k_{Δ} and k_{Δ} ' values are negligible, dividing eq. 104 by eq. 103 gives:

$$\frac{n_{u}'}{n_{u}} = \left[\frac{(1 - \chi_{a})n_{e(a)} + (1 - \chi_{m})n_{e(m)} + (1 - \chi_{Ar})n_{e(Ar)}}{(1 - \chi_{a})n_{e(a)} + (1 - \chi_{Ar})n_{e(Ar)}} \right] x$$

$$\left[\frac{k_{hv} + k_{CD} \left((1 - \chi_{a})n_{e(a)} + (1 - \chi_{Ar})n_{e(Ar)} \right) + k_{CT}' \left(n_{+(a)} + n_{+(Ar)} \right)}{k_{hv} + k_{CD} \left((1 - \chi_{a})n_{e(a)} + (1 - \chi_{m})n_{e(m)} + (1 - \chi_{Ar})n_{e(Ar)} \right) + k_{CT}' \left(n_{+(a)} + n_{+(Ar)} + n_{+(m)} \right)} \right]$$
(105)

The ambipolar diffusion ion-pair complex is stabilized by resonance as follows:

 $M \leftrightarrow [M^{^+}e^{^-}] \leftrightarrow M^{^+} + e^{^-},$ as well as by electrostatic attraction.

If we assume:

 $\chi_{Ar}\approx$ 1, $\chi_{a}\approx$ 0, and $\chi_{m}\approx$ 0, then eq. 105 can be written as:

$$\left[\frac{n_{e(a)} + n_{e(m)}}{n_{e(a)}}\right] \left[\frac{k_{hv} + k_{CD}n_{e(a)} + k_{CT}'(n_{+(a)} + n_{+(Ar)})}{k_{hv} + k_{CD}(n_{e(a)} + n_{e(m)}) + k_{CT}'(n_{+(a)} + n_{+(Ar)} + n_{+(m)})}\right]$$
(106)

If we further assume that charge transfer involving analyte ions and activated Ar atoms is negligible because of the high activation energy required (\sim 15.7 eV), and that $n_{e(m)}$ (= $n_{+(m)}$) >> $n_{e(a)}$ (= $n_{+(a)}$) then eq. 106 can be written as

$$\frac{n_{u}'}{n_{u}} = \left[\frac{n_{m+}}{n_{+}}\right] \left[\frac{k_{hv} + k_{CD}n_{+}}{k_{hv} + k_{CD}n_{m+}}\right]$$
(107)

Eq. 107 shows that 4 limiting cases can be identified depending on whether $k_{CD}n_+$ and $k_{CD}n_{m+}$ are greater or less than $k_{h\nu}$ thus:

<u>Limiting Case IIA. Low analyte, low interferent:</u>

$$(k_{CD}n_{+} << k_{hv} >> k_{CD}n_{m+})$$

$$\frac{n_u'}{n_u} = \frac{n_{m+}}{n_+} \tag{108}$$

i.e., at very low concentrations of analyte and interferent, the observed signal enhancement will be directly proportional to interferent concentration, and inversely proportional to the concentration of the analyte.

<u>Limiting Case IIB. High analyte, low interferent:</u>

 $(k_{CD}n_{+} >> k_{hv} >> k_{CD}n_{m+})$

$$\frac{n_u'}{n_u} = \frac{k_{CD} n_{m+}}{k_{hv}} \tag{109}$$

i.e., at very high concentrations of analyte and low interferent concentrations, the observed signal enhancement will be directly proportional to interferent concentration, but independent of the concentration of the analyte.

<u>Limiting Case IIC. Low analyte, high interferent:</u>

 $(k_{CD}n_{+} << k_{hv} << k_{CD}n_{m+})$

$$\frac{n_u'}{n_u} = \frac{k_{hv}}{k_{CD}n_+} + 1 \tag{110}$$

i.e., at very low concentrations of analyte and high interferent concentrations, the observed signal enhancement will be inversely proportional to analyte concentration, but independent of interferent concentration.

<u>Limiting Case IIC. High analyte, high interferent:</u>

$$(k_{CD}n_{+} >> k_{hv} << k_{CD}n_{m+})$$

$$\frac{n_u'}{n_u} = 1 \tag{111}$$

i.e., at high concentrations of analyte and high interferent concentrations, no signal enhancement will be observed.

Figures 3 and 4 show the typical E'/E curve obtained for the effects of excess Li and K on the line emission of Call, MgII, and SrII. It is apparent from these curves that eq. 110 correlates with the portion of the curve below about 1 µg/mL analyte, while eq. 111 correlates with the curve above 1 µg/mL analyte.

4.3 Simulating the Experimental curve: Use of apparent rate constants

Simulation of the E'/E curve can be achieved provided we can identify the limiting case we are dealing with in terms of concentration of the analyte and interferent as discussed. However, before we can be able to do so, we must compute the values for k_{hv} and k_{CD} .

4.3.1 Estimation of k_{hv}

The rate constant for radiative relaxation, $k_{h\nu(\psi 2 \to \psi 1)}$, is given by [100]:

$$k_{hv(\psi_2 \to \psi_1)} = (\sigma_{\text{max}})^2 f / 1.5$$
 (111)

where σ_{max} is the wavenumber for the maximum wavelength, λ , of the emission, and f is the oscillator strength.

The wavenumber associated with 1 eV, s_0 , is 8066.02 \pm 0.14 cm⁻¹. Assuming $f \cong 1$, for K, $\Delta E = 1.6275$ eV,

$$k_{h\nu(\psi_2 \to \psi_1)} = 1.1489 \, x \, 10^8 \,, \tag{112}$$

It can be shown that the values of k_{hv} for Call, MgII, and SrII are 4.3098 x 10⁸, 8.531 x 10⁸ and 4.0095 x 10⁸, respectively (corresponding to the 393.3-nm line(Call), 279.553 nm line (MgII), 407.771 nm line (SrII) and 766.5 nm line (KI) respectively), see Table 14.

4.3.2Theoretical calculations number densities and rate constants

4.3.2.1 Calculation of number densities

The number density of metal species in the plasmas, e.g. for Ca species, is a product of:

{mass of Ca aspirated by nebulizer (m) X nebulization efficiency (ξ) X conversion factor from mass to mole for Ca X Avogadro's number (Na) X carrier gas volumetric flow rate (F_c) X expansion factor of carrier gas from room temperature to the plasma temperature (χ)}, i.e.:

$$n_M = \frac{\xi N_a qc}{mF_c \chi} \tag{113}$$

where $\chi = T_a/T_{init}$ (= 20 for Ca species) in which T_i in the initial temperature of the carrier gas and T_a is the absolute temperature. The estimated number density of Ca at an assumed plasma temperature at 9000 K is given by:

$$c(mg) Ca/L x 5\% x \frac{1 mole}{40 g Ca} x 6.02 x 10^{23} / mole x \frac{1}{1L Ar/\min} x \frac{300 K}{9000 K}$$

$$= c \mu g Ca/mL x 1 mL/\min x 0.05 x \frac{1 mole}{40 g Ca} x 6.02 x 10^{23} / mole x \frac{1}{1000 cm^{-3} Ar/\min} x \frac{1}{30}$$

$$= c x 10^{-6} g Ca/mL x 1 mL/\min x 0.05 x \frac{1 mole}{40 g Ca} x 6.02 x 10^{23} / mole x \frac{1}{1000 cm^{-3} Ar/\min} x \frac{1}{30}$$

$$= 2.51 x 10^{10} c/cm^{3} Ar$$

$$(114)$$

The values obtained for the species under study are shown in Table 15 and 16 for the ICP and Flame experiments respectively.

4.3.2.2 Calculation of the degree of ionization

The degree of ionization for Li and K were calculated using the Saha equation, (given in eqns 66 and 67). The values obtained were in excess of ground state number densities, implying close to 100% ionization. The Literature values in Table (16) and Table (17) for Mg, Ca and Sr were used.

For the air-acetylene flame experiments, flow number densities were calculated assuming 4.0±0.1 g/min. aspiration rate, and 5.7±0.2% nebulization efficiency (see Experimental section), and 2573 K temperature.

Table 14. Values of $\Delta E,\,k_{\!\scriptscriptstyle \Delta}$ and $k_{\!\scriptscriptstyle hv}$ for CaII, MgII, SrII, and K

M	ΔE (eV)	g u	g _o	${\sf k}_{\!\scriptscriptstyle\Delta}$	k _{hv}	
	ICP I	Experim	nents			
Cal Call MgII SrII	2.933 3.152 4.435 4.009	3 4 4 4	1 2 2 2	2.28 e-2 3.43 e-2 6.57 e-3 3.97 e-2	3.73 e+8 4.31 e+8 8.53 e+8 4.01 e+8	
Air-acetylene Experiments						
K	1.618	4	2	6.787 e-4	1.13e+8	
Mg	1.848	4	2	2.394 e-4	1.48e+8	

Table 15. Number densities: ICP experiments

M			Number densities	s (atoms/ions	cm ⁻³ s ⁻¹)
	[MI]	(Desig)	[MII]	(Desig)	n _(a2+)
Ca	2.52x10 ¹⁰ c	(n _(a))	2.46 x10 ¹⁰ c	$(n_{(a+)})$	1.58 x 10 ⁹ c
Mg	4.10x10 ¹⁰ c	(n _(a))	3.81x10 ¹⁰ c	(n _(a+))	2.45 x 10 ⁹ c
Sr	1.13x10 ¹⁰ c	(n _(a))	1.13x10 ¹⁰ c	$(n_{(a+)})$	2.23 x 10 ⁹ c
Ar	2.69x10 ¹⁹	(n _(Ar))	2.92x10 ¹⁶	$(n_{(Ar+)})$	
Li	1.44x10 ¹⁴	(n _(m))	1.44x10 ¹⁴	(n _(m+))	
K	2.55x10 ¹³	(n _(m))	2.55x10 ¹³	(n _(m+))	

M = element; Desig = designation

Table 16. Number densities: Air-acetylene flame experiments

M	Flow number densities (atoms/ions cm ⁻³ s ⁻¹)					1 ⁻³ s ⁻¹)
	[MI] cm ⁻³	(Desig)	[MII] cm ⁻³	(Desig)	α	β
K	1.78 x 10 ¹¹ c	(n _(a))	1.96 x 10 ⁹ c	$(n_{(a+)})$	0.011	
Mg	$9.73 \times 10^{12} c$	(n _(a))	4.86 x 10 ⁹ c	$(n_{(a+)})$	0.005	84%
Li	1.00 x 10 ¹⁵	(n _(m))	2.81 x 10 ¹³	$(n_{(m+)})$	0.028	
Na	3.03 x 10 ¹⁴	(n _(m))	2.82 x 10 ¹³	(n _(m+))	0.093	
K	1.78 x 10 ¹⁴	(n _(m))	1.96 x 10 ¹²	(n _(m+))	0.011	

M = element; Desig = designation; α = degree of ionization; β = atomization efficiency [61].

Table 17. Values of M^+/M (Experimental at 1 KW rf power) and M^{2^+}/M^+ (Theoretical at 9000 K) for Mg, Ca and Sr.

Element	M ⁺ /M (%)*	M^{2+}/M^{+} (%)**	
Mg	93.0	0.174	
Mg Ca	98.9	6.43	
Sr	99.4	19.7	

Source: *[120]; **[139]

4.3.2.3 Empirical values of kcD

If, from equation (99d), we further assume experimental conditions such that $k_{CD}n_+>>k_{hv}\ \ {\rm then,\ the\ equation\ further\ simplifies\ to:}$

$$\frac{n_u'}{n_u} = \frac{n_{m_+}}{n_+} \left[\frac{k_{hv} + k_{CD} n_+}{k_{CD} n_{m_+}} \right]$$

$$\frac{E'}{E} = 1 + \frac{k_{hv}}{k_{CD}n_+}$$

(115)

Therefore a plot of E'/E vs k_{hv} / n_+ , will give a slope = $1/k_{CD}$. Using E'/E data from Chapter 2, the various values of k_{CD} obtained from the plots for the analytes and interferents under study are shown in Table 18.

Table 18. k_{CD} values, ICP and Flame Experiments .

ICP Measurements.

Analyte / Intereferent	Intercept	1/k _{CD}	k _{CD}
MgII / K	1.0239	38.9754 r ² = 0.9898	2.566e-2
MgII / Li	1.0049	$39.7844 r^2 = 0.990$	2.514e-2
Call / Li	0.91274	57.0104 r ² = 0.9528	1.754e-2
SrII / K	1.04561	33.0678 r ² = 0.9132	3.024e-1
Srll / Li	1.02122	34.0898 r ² = 0.9790	2.933e-2
Mean Intercept value	1.002		

Flame Measurements.

	1.742 5.215e-3 = 0.716
--	---------------------------

When the values of k_{CD} in the Table 16 are substituted into eq. 106 the following equations for n_u '/ n_u are obtained:

For CaII/Li

$$\left(\frac{n_u'}{n_u'}\right)_{Call/Li} = 1 + \frac{(4.3098 \times 10^8)(57.0104)}{2.46 \times 10^{10} c}$$

$$= 1 + 9.988 \times 10^{-1}/c$$
(116)

For MgII/K

$$\left(\frac{n_u'}{n_u}\right)_{MgII/K} = 1 + \frac{(5.831x10^8)(38.975)}{3.8134x10^{10}c}$$

$$= 1 + 5.960x10^{-1}/c$$
(117)

For MgII/Li

$$\left(\frac{n_u'}{n_u}\right)_{Mg/Li} = 1 + \frac{(5.831x10^8)(39.7844)}{3.8134x10^{10}/c}$$

$$= 1 + 6.083x10^{-1}/c$$
(118)

For SrII/Li

$$\left(\frac{n_u'}{n_u}\right)_{SrII/Li} = 1 + \frac{(4.0095 \, x \, 10^8)(34.0899)}{1.1309 \, x \, 10^9/c}$$

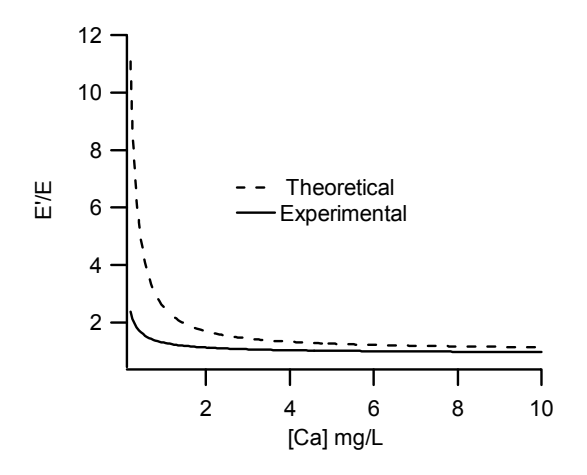
$$= 1 + 12.09/c \tag{119}$$

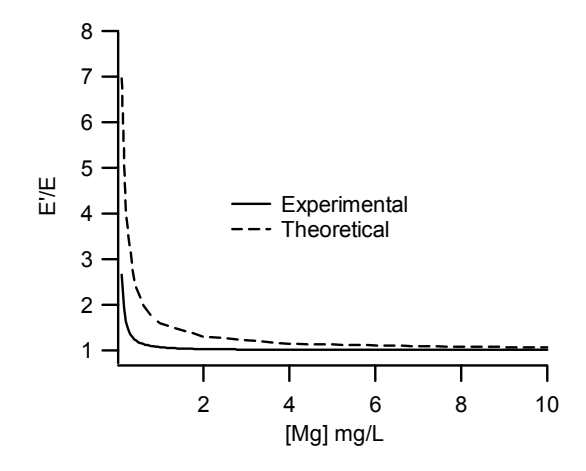
For (Mg/K)_{Flame}

$$\left(\frac{n_u'}{n_u}\right)_{Mg/K} = 1 + \frac{(1.1348 \times 10^8)(191.7422)}{2.5495 \times 10^{11}/c}$$

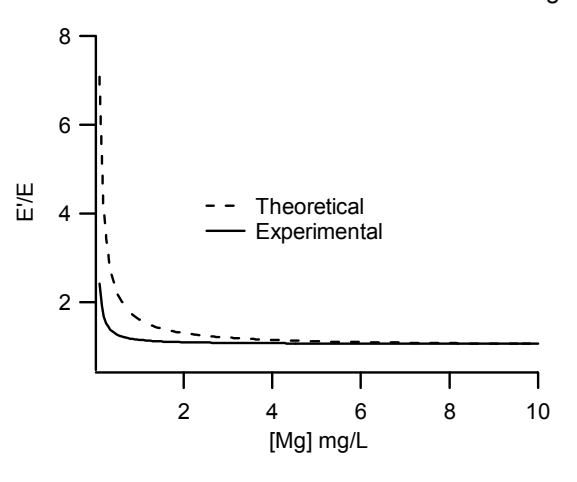
$$= 1 + 8.535 \times 10^{-2}/c$$
(120)

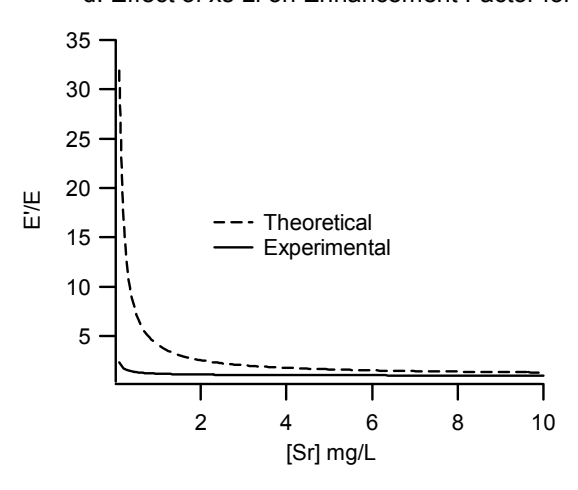
- a. Effect of xs Li on Enhancement Factor for Call
- b. Effect of xs K on Enhancement Factor for MgII





- c. Effect of xs Li on Enhancement Factor for MgII
- d. Effect of xs Li on Enhancement Factor for Srll





e. Effect of xs K on Enhancement Factor for MgI, flame exp

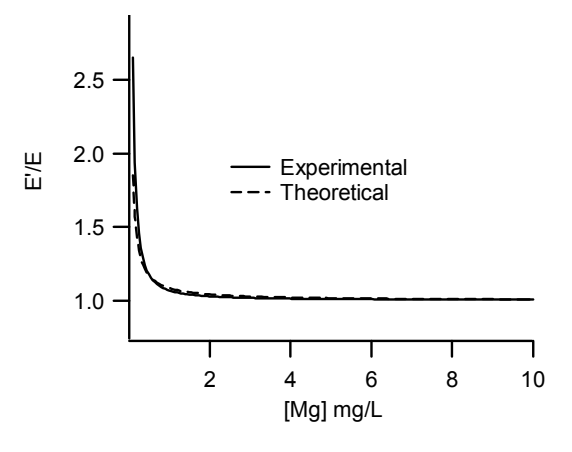


Fig. 12 (a-d) Effect of 1000 mg/L Li/K on Ca, Mg and Sr ion line emission intensity (ICP exp. (e) Effect of 1000 mg/L K on Mgl line emission. (Data for the plots are shown in Tables 3, 5, 6 7 and 8. Data points were limited to 10 mg/L [Ca] in order to illustrate more clearly the region where change is occurring).

The plots of E'/E in Fig. 12 show that the theoretical curves derived using equation 106 resemble the experimental curves in shape. However, the theoretical values generally exceed the experimental values in all cases. Also, the behaviour of the theoretical curves for Call, MgII, and SrII (Fig. 12a-d) in the region of interest (<1 mg/L) are different from the experimental ones with E'/E values dropping more rapidly with [Ca] than n_u'/n_u values. However, the model appears to predict quite well the experimental data for the effect of K on MgI emission line during flame experiments (Fig. 12e).

The differences between the theoretical and experimental curves for the ICP experiments can be explained in terms of the assumptions made in deriving eqn 106. The assumptions made is that $k_{CD}n_{+} >> k_{hv}$. Substitution of appropriate values for the MgII/K (as an example) shows that $(k_{CD}n_{+} = 6.446 \times 10^{8} \text{c})$ vs $k_{hv} = 8.531 \times 10^{8}$ does not satisfy the assumption in the analyte concentration range covered (0.1-10 mg/L). For the flame experiments, however, it can be shown that $k_{CD}n_{+} = (5.072 \times 10^{10}) > k_{hv} = (1.4821 \times 10^{8})$, which may explain the agreement between the theoretical and experimental values for the flame experiments.

Rearrangement of equation (106) yields:

$$k_{\rm CD} = \frac{k_{\rm hv}}{\left(E'/E-1\right)\!n_{\scriptscriptstyle +}}$$
, showing that for a given transition, k_{CD} increases with

decreasing n_+ , thus the effect would be to decrease E'/E ratios. The equation also shows that k_{CD} values are independent of interferent concentration, for the situation of high interferent/low analyte concentration. An interesting point to note is that Tables of k_{CD} empirical values can be obtained for specifically designed

experimental conditions, which can be useful in coming up with modified calibration curves, thus coming up with another alternative for correcting for the matrix effects.

The major findings in this chapter were that:

- (a). the spatial variation of emission signal enhancement in the presence of an easily ionizable element depended on the analyte ion number density, n_+ and collisional deactivation rate constant, k_{CD} .
- (b). based on the assumption; $\chi_{Ar}\approx 1$, $\chi_a\approx 0$, $\chi_m\approx 0$, the ambipolar diffusion model successfully predicted the experimental curve of emission enhancement vs analyte concentration.
- (c). it is possible to obtain empirical values of k_{CD} for specifically designed experimental conditions which can be tabulated and used in matrix effects correction.

CHAPTER 5: CONCLUSIONS AND RECOMMENDATIONS FOR FUTURE WORK

5.1 Conclusions

Emission signal intensities were measured for MgII, Call, SrII, during ICP determination and for MgI and KI during Flame AES in the presence and absence of interferent elements. The results showed a pronounced emission signal enhancement due to the presence of the EIEs. The experimental results have been interpreted in terms of two possible simplified models: a collisional rate model based on ambipolar diffusion and a model based on charge transfer between analyte and interferent. A similarity between the curves for flame AES and ICP-OES suggested that the contribution of charge transfer process involving Ar species on analyte excitation was negligible under the experimental conditions employed in the ICP. The ambipolar diffusion model successfully predicted the experimental curve of emission enhancement vs analyte concentration and showed that the spatial variation of emission signal enhancement in the presence of an easily ionizable element depended on the analyte ion number density, n+ and collisional deactivation rate constant, k_{CD} . Trends in which ion emission is enhanced off-axis and depressed on-axis can be explained in terms of the ambipolar diffusion model, by considering how the analyte ion number density, n₊ varies with spatially. The simplified rate model was used to derive empirical values of k_{CD} and these values were found to vary inversely with analyte ion concentration, thus suggesting that k_{CD} is dependent on analyte ion concentration. The results also show that simplified rate models can be used to obtain empirically derived k_{CD} values which can be tabulated for various elements and interferents for specified experimental conditions and used in plotting calibration curves corrected for the effect of easily ionizable elements. However although the model shows reasonably good agreement for the effect of K on MgI emission, it does not appear to show such agreement for the ICP studies. The simplified rate model showed that k_{CD} values were independent of interferent concentration. More work is needed to establish the relationship between k_{CD} values and interferents, since different interferents would be expected to cause different emission signal enhancement effects. The charge transfer model showed that effect of easily ionized elements during ICP-AES and flame AES can be described using a simplified rate model based on collisional charge transfer between analyte and interferent species for analyte concentration range under study. Theoretical calibration curves derived on the bases of the simplified model showed good agreement with experimental curves. The model also showed that it possible to explain the spatial variation of emission signal enhancement by considering how the degree of ionization varies spatially. Lastly, the model highlighted possibility of obtaining values of thermal excitation rate constant, k_{Δ} , for a given analyte-interferent combination experimentally. However, we should point out that the simplified rate model as presented in this thesis, may not tell the full story as far as mechanisms of excitation in flame AES or ICP-OES are concerned, but the fact that it leads to close simulation of the analytical calibration curve obtained in the presence of easily ionized interferents is of significance.

5.2 Recommendations for future work

The work presented in this thesis is quite limited in a number of ways. The simplified rate models derived focused on only one particular energy level, namely the upper energy level of Ca II, Mg II, and Sr II for ICP and K I (for flame) emission lines that were measured. It would be desirable, that further work be carried out involving as many transitions as possible. It would be interesting also to investigate variation of E'/E ratios with height above load coil, and to carry out spatial mapping. The model should be tested on more matrix/analyte combinations, to check the assumptions on a more general basis. Future simplified rate modeling would also benefit from kinetic simulation software to optimize the estimated parameters and to simulate the experimental curves.

REFERENCES:

- Gregoire, D. C. (1987), Non-spectroscopic interferences in ICP-MS.
 Spectrochim Acta, 42B (7), 895-907.
- Douglas, D. J and Tanner, S. D (1998), in "Inductively Coupled Plasma
 Mass Spectrometry". Ed. A. Montaser, Wiley-VCH, New York, 615.
- 3. Hill, S. J (1999), *Inductively Coupled Plasma Spectrometry and Its*Applications, Sheffield Academic Press, Sheffield, p 1.
- 4. Boumans, P. W. J. M (1987), *Inductively Coupled Plasma Emission*Spectroscopy, Part 2. Applications and fundamentals, John Wiley and Sons,

 New York, p 486.
- 5. Hieftje, G. M and Vickers, G. H (1989), *Developments in plasma* source/mass spectrometry, Anal. Chim. Acta (216), 16, 1-24.
- 6. Boorn, A. W and Browner, R. F (1987), *In Inductively Coupled Plasma Emission Spectroscopy. Part II*, ed. P. W. J. M. Boumans, John Wiley and Sons, New York, p. 151.

- 7. Mermet, J. M (1998), Re-visitation of the matrix effects in inductively coupled plasma atomic emission spectrometry: the key role of the spray chamber, J. At. Spectrom., 419-426.
- 8. Todolı´, J. L, Gras, L, Hernandis, V and Mora, J (2002), *Elemental matrix* effects in ICP-AES, Review, J. Anal. At. Spectrom, 17, 142–169.
- Nikdel, S and Winefordner, J. D (1980), Interference of potassium on barium measurements in the inductively coupled plasma, Microchem. J (25), 2, 254-256.
- 10. Hoenig, M (2001), Preparation steps in environmental trace element analysis-facts and traps, Talanta (54), 6, 1021-1038.
- Pritchard, E, McKay, G. H and Points, J (1996), Trace Analysis. A
 Structured Approach to Obtaining Reliable Results, Royal Society of Chemistry, Cambridge, p 1.
- Evans, E. H, Dawson, J. B, Fisher, A, Hill, S. J, Price, J. W, Smith, C. M. M, Suttone, K. L and Tyson, J. F (2001), Atomic Spectrometry Update.
 Advances in atomic emission, absorption, and fluorescence spectrometry, and related techniques, J. Anal. At. Spectrom., 16, 672–711.

- 13. Thompson, M and Ramsey, M. H (1985), *Matrix effects due to calcium in inductively coupled plasma atomic emission spectrometry: their nature, source and remedy,* Analyst, 110, 1413-1422.
- Hieftje. G. M, Huang. M, Lehn S., Warner. K, Gamez. G, Ray. S and Leach.
 A (2002), Toward a Fuller Understanding of Analytical Atomic Spectrometry,
 Anal. Sciences, Reviews18, 1185-1189.
- Gine', M. F, Bergamin, H, Reis, B. F, Tuon, R. L (1990), *Intelligent flow-injection-inductively coupled plasma system for matrix matching*, Anal.
 Chim. Acta, 234, 207-212.
- 16. Horner, J. A, Hieftje, G. M (1998). Computerized Simulation Of Mixed-Solute Particle Vaporization in an Inductively Coupled Plasma.

 Spectrochim. Acta 53B, 1235-1259.
- 17. Boumans, P. W. J. M (1966), *Theory of Spectrochemical Excitations*, Higler and Watts, London, p 317.
- Mermet, J. M (1987), Spectroscopic Diagnostics: Basic Concepts in Inductively Coupled Plasma Emission Spectroscopy, ed. P. W. J. M. Boumans, John Wiley and Sons, New York, p. 353.

- Sesi, N. N, Hanselman, D. S, Galley, P, Horner, J, Huang, M, Hieftje G. M
 (1997), An imaging based instrument for fundamental plasma studies,
 Spectrochim. Acta 52B, 83-102.
- 20. Boumans, P. W. J. M (1987), *Inductively Coupled Plasma Emission*Spectroscopy, Part 1, John Wiley and Sons, New York, p 1.
- Sengoku, S and Wagatsuma, K (2006), Comparative Studies of
 Spectrocheical Characteristics between Axial and Radial Observations in
 Inductively Coupled Plasma Optical Emission Spectrometry, Anal. Sciences.
 22, 245-249.
- Sesi, N. N. and Hieftje, G. M (1996), Studies into the Inter-element Matrix
 Effect in Inductively Coupled Plasma Spectrometry. Spectrochim. Acta, 51B (13), 1601-1628.
- Vicek, J and Pelikan, V (1992), Collisional-radiative ionization and recombination in inductively coupled argon plasma, Spectrochim. Acta 47B (5), 681-688.
- 24. Olesik, J. W and Bradley, K. R (1987), *Analyte excitation in the inductively coupled plasma studied by power modulation,* Spectrochim. Acta 42B (1-2), 377-392.

- Furuta, N (1986), Spatial emission distribution of YO, YI, YII radiation in an inductively coupled plasma for the elucidation of excitation mechanisms, Spectrochim. Acta, 41B (10), 1115-1129.
- 26. Mostaghimi, J, Proulx, P and Boulos, M. I (1985), Computer modeling of the emission pattern for a spectrochemical ICP, Spectrochim. Acta 52B, 120-133.
- 27. Gillson, G and Horlick, G (1986), *An atomic absorption study of ground state*neutral atoms and ions in the inductively coupled plasma, Spectrochim.

 Acta: Atomic Spectroscopy 41B (5), 431-438.
- 28. Wagatsuma, K and Hirokawa, K (1993), Assessment of the population of neutral and singly ionized zinc species in argon and argon-nitrogen inductively coupled plasma by atomic absorption spectrometry, Anal. Chim. Acta (284), 2, 351-360.
- 29. Lehn, S. A, Huang, M, Warner, K. A, Gamez, G and Hieftje, G. M (2003), Spatially resolved ground-state number densities of calcium and strontium ion in an inductively coupled plasma in contact with an inductively plasma mass spectrometry sampling interface, Spectrochim. Acta, (58B) 9, 1647-1662.

- 30. Lehn, S. A. and Hieftje, G. M (2003), Experimental Evaluation of Analyte

 Excitation Mechanisms in the Inductively Coupled Plasma. Spectrochim.

 Acta, Part B, 58(10), 1821-1836.
- 31. Blades. M. W and Horlick. G (1981), Interference from easily ionisable element matrices in inductively coupled plasma emission spectrometry a spatial study, Spectrochim Acta 36B (9), 881-900.
- 32. Montaser, A and Golightly, D. W (1988), *Inductively coupled plasmas in analytical atomic spectrometry*, Microchem. J. (38), 2, 278-279.
- Montaser, A and Golightly, D. W (1988), Inductively coupled plasmas in analytical atomic spectrometry, Geochim. et Cosmochim. Acta (52), 4, 951-966.
- Horlick, G and Shao, Y (1992), in Inductively Coupled Plasmas in Analytical Spectrometry, ed. A. Montaser, VCH Publishers, New York, 2nd edn., p. 571.
- 35. Montaser, A, Minnich, M. G, McLean, J. A, Liu, H, Caruso, J. A and McLeod, C. W (1998), in Inductively Coupled Plasma Mass Spectrometry, ed. A. Montaser, Wiley-VCH, New York, p 1.

- 36. Mermet, J. M (1999), Fundamental Principles of Inductively Coupled

 Plasma, in Handbook of ICP Spectrometry, ed. S. Hiel, Sheffield Academic

 Press, Sheffield, p. 35.
- 37. Dymott, T.C (1989), Source Design in Inductively-Coupled Plasma/Optical Emission Spectrometry, International Laboratory, 19 (7), 33-43.
- Furuta, N (1985), Spatial profile measurement of ionization and excitation temperatures in an inductively coupled plasma. Spectrochim. Acta 40B (8), 1013-1022.
- 39. Ingle, J. D Jr and Crouch, S. R (1988), *Spectrochemical analysis,* Prentice-Hall, Englewood Cliffs, New Jersey, p 235-136.
- 40. Haraguchi, H (1986), *In Inductively Coupled Plasma Atomic Emission*Spectrometry-Fundamentals and Applications; Kodansha Scientific Publishers: Tokyo, p 1.
- 41. Blades, M. W. and Hieftje, G. M. (1982), *On the Significance of Radiation Trapping in the Inductively Coupled Plasma*. Spectrochim. Acta 37B, 191197.

- 42. Gunter. W, Visser. K, and Zeeman. P. B (1985), Ionization interferences under various operating conditions in an 9, 27 and 50 MHz ICP, and a study of shifts in level populations of calcium through simultaneous absorption-emission measurements in a 9 MHz ICP, Spectrochim. Acta, 40B (4), 617-629.
- Galley, P. J, Glick, M., and Hieftje, G. M (1993), Easily Ionizable Element
 Interferences in Inductively Coupled Plasma Atomic Emission Spectroscopy
 - I. Effect on Radial Analyte Emission Patterns. Spectrochim. Acta 48B,
 (6/7), 769-788.
- 44. Galley, P.J and Hieftje, G.M (1994). Easily Ionizable Element Interferences in ICP-AES Part II. Minimization of EIE Effects by Choice of Observation Volume. Spectrochim. Acta 49B (7), 703-724.
- 45. Van der Sande, M. J, van Eck. P, Sola. A and van der Mullen. J.J.A.M (2002), The relation between internal and external parameters of a spectrochemichal inductively coupled plasma, Spectrochim Acta 57B, 829-842.
- 46. Boumans, P. W. J. M and de Boer. F. J (1977), An experimental study of a 1 kW, 50 MHz RF inductively coupled plasma with pneumatic nebulizer and a discussion of experimental evidence for a non-thermal mechanism, Spectrochim. Acta 32B, 365-395.

- 47. Yang. P, Wang. X, Ying. H, Deng. Z, Wang. Z (1993), *Non-local thermal equilibrium in ICP-AES-non Boltzman distribution in excitation,* Spectrosc. Spectrom. Anal. (China), 5, 63-68.
- 48. Mingzhao, L and Zhanxia, Z (1998), Study on the excitation mechanism 1.

 Non-Boltzmann-Saha distributions in the inductively coupled plasma.

 Spectrochim Acta 53B, 1391-1398.
- 49. Boumans, P. W. J. M and De Boer, F. J (1977), An experimental study of a 1-kW, 50-MHz RF inductively coupled plasma with pneumatic nebulizer, and a discussion of experimental evidence for a non-thermal mechanism, Spectrochim. Acta 32B, (9/10), 365-395.
- 50. Rayson, G. D and Hieftje, G. M (1985), A steady-state approach to evaluation of proposed excitation mechanisms in the analytical ICP, Spectrochim Acta 41B (7), 683-697.
- 51. Alder J. F, Bombelka R. M. and Kirkbright G. F (1980), *Electron excitation*and ionization temperature measurements in high-frequency inductively

 coupled plasma source and the influence of water-vapour on plasma

 parameters. Spectrochim Acta 35B, 163-175.

- 52. Hanselman, D. S, Sesi, N. N, Huang, M, and Hieftje, G. M (1994), The Effect of Sample Matrix on Electron Density, Electron Temperature and Gas Temperature in the Argon Inductively Coupled Plasma Examined by Thomson and Rayleigh Scattering. Spectrochim. Acta. Electron., 49(5), 495-526.
- 53. Mermet, J. M (1989), *lonic to atomic line intensity ratio and residence time in inductively coupled plasma-emission spectrometry,* Spectrochim. Acta. 44B (11), 1109-1116.
- 54. Nowak, S, Van Der Mullen, J. A. M and Schram, D. C (1988), *Electron density and temperature determination in an ICP using a non-equilibrium concept*, Spectrochim. Acta 43B, (9/11), 1235-1245.
- 55. Galley, P. J and Hieftje, G. M (1993), Tomographically Resolved Ionization

 Temperatures and Electron Densities in the Inductively Coupled Plasma

 Determined by the Line to Continuum Method. Spectrochim. Acta 48B,

 E1725-E1742.
- Hieftje, G.M, Galley, P.J, Glick. M, and Hanselman, D. S (1992), New
 Developments and Final Frontiers in Inductively Coupled Plasma
 Spectrometry. J. Anal. At. Spectrom., 7, 69-73.
- 57. Huang, M. and Hieftje, G. M (1985), *Thomson Scattering from an ICP.*Spectrochim. Acta 40B, 1387-1400.

- 58. Marshall, K. A and Hieftje, G. M (1988), Thomson Scattering for

 Determining Electron Concentrations and Temperatures in an ICP I.

 Assessment of the Technique for a Low-Flow, Low-Power Plasma.

 Spectrochim. Acta 43B, 841-849.
- Monning, C.A., Marshall, K.A., Rayson, G.D., and Hieftje, G.M (1988),
 Tomographic Image Reconstruction Techniques for Spectroscopic
 Sources: 1. Theory and Computer Simulations. Spectrochim. Acta 43B,
 1217-1233.
- 60. Hieftje. G.M (1992), *Plasma Diagnostic Techniques for Understanding and Control.* Spectrochim. Acta 47B, 3-25.
- 61. Willard, H. H, Merritt, L. L, Dean, J. A, Settle, F. A, Jr (1988), *Instrumental Methods of Analysis*, 7th ed., Wadsworth, p 232.
- 62. Prell. L.J, Monning. C., Harris. R.E. and Koirtyohann (1985), *The role of electrons in the emission enhancement by easily ionized elements low in the inductively coupled plasma*. Spectrochim. Acta 40B (10), 1401-1410.
- 63. Hartgers, A and van der Mullen, J. J. A. M (2001), Modelling an Ar-Hg fluorescent lamp plasma using a 3 electron-temperature approximation, J. Phys. D: Appl. Phys., 34, 1907-1913.

- 64. Moisan, M, Hubert, J, Margot, J, Sauve, G and Zakrzewski, Z (1993), The contribution of surface-wave sustained plasmas to hf plasma generation, modeling and applications: status and perspectives, in: C. Ferreira, M. Moisan (Eds.), Microwave discharges: fundamental and applications, Plenum Press, New York, p 1.
- 65. Ferreira, C. M and Moisan, M (1988), The similarity laws for the maintenance field and the absorbed power per elecetron in low-pressure surface wave produced plasmas and their extension to hf plasmas in general, Physica Scripta, 38, 383.
- de Regt, J. M, Tas, R. D, van der Mullen, J. J. A. M, and Schram, D. C
 (1996), A closed inductively coupled plasma for lighting purposes mapped
 by spectroscopical techniques, J. Phys. D. Appl. Phys., 29, 1489-1496.
- 67. Huang, M., Marshall, K. A., and Hieftje, G. M (1986), *Electron Temperatures* and *Electron Number Densities Measured by Thomson Scattering in the Inductively Coupled Plasma.* Anal. Chem., 58, 207-210.
- 68. Huang, M and Hieftje, G. M (1989). A New Procedure for Determination of Electron Temperatures and Electron Concentrations by Thomson Scattering from Analytical Plasmas. Spectrochim. Acta 44B (3), 291-305.

- 69. Huang, M and Hieftje, G. M, (1989), Simultaneous Measurement of Local Electron Temperatures, Electron Number Densities and Gas Temperature by Laser Light Scattering from the ICP. Spectrochim. Acta, Part B, 44B(8), 739-749.
- 70. Huang, M, Hanselman, D. S., Yang, P, and Hieftje, G. M (1992). *Isocontour Maps of Electron Temperature, Electron Number Density and Gas Kinetic Temperature in the Ar Inductively Coupled Plasma Obtained by Laser-Light Thomson and Rayleigh Scattering.* Spectrochim. Acta 47B (6), 765-785.
- 71. van der Mullen and Jonkers. J (1999), Fundamental comparison between non-equilibrium aspects of ICP and MIP discharges, Spectrochim. Acta 54B, 1017-1044.
- 72. Huang. M, Yang. P. Y, Hanselman. D. S, Monning. C. A, and Hieftje. G. M (1989), *Verification of a Maxwellian electron-energy distribution in the ICP,* Spectrochim. Acta 45B, 511-520.
- 73. Huang, M, Lehn, S. A, Andrews, E. J, and Hieftje, G. M (1997), Comparison of Electron Concentrations, Electron Temperatures, Gas-Kinetic Temperatures, and Excitation Temperatures in Argon ICPs Operated at 27 and 40 MHz. Spectrochim. Acta 52B (8), 1173-1193.

- 74. de Regt. J. M, Engeln. R. A. H, de Groote. F. P. J, van der Mullen. J. J. A.
 M, and Schram. D. C (1995), Thompson scattering with Raman Scattering
 Calibration, Rev. Sci. Inst. 66, 3228-3235.
- 75. de Regt. J. M, Tas. R. D, van der Mullen. J. J. A. M (1996), *A diode laser* absorption study on 100 MHz argon inductively coupled plasma, J. Phys. D: Appl. Phys., 29, 2404-2410.
- 76. de Regt. J. M, de Groote. F. P. J, van der Mullen. J. J. A. M, Schram. D. C (1996), Comparison of active and passive spetroscopic methods to investigate atmospheric inductively coupled plasmas, Spectrochim. Acta 51B, 1371-1383.
- van der Mullen. J. J. A. M and de Regt (1996), *An active spectroscopical study on the plasma parameters of an ICP,* Fresenius J. Anal. Chem., 355, 532-542.
- Jonkers. J, Selen. L. J. M, van der Mullen. J. J. A. M, Timmermans. E. A. H,
 Schram. D. C (1997), Steep plasma gradients studied with spatially resolved
 Thomson Scattering Measurements, Plasma sources Sci. Technol., 6, 533-561.
- 79. Kempkens. H and Uhlenbusch. J (2000), Scattering diagnostics of low-temperature plasmas (Rayleigh Scattering, Thomson Scattering, Cars), Plasma Sources Sci. Technol., (9), 492-500.

- 80. DeSilva. A. W, Goldenbaum. G. C (1970), *Plasma diagnostics by light*scattering, in: H. Griem, R. Lovberg (Eds.), Methods of Experimental Physics, 9A, Academic Press, New York, p. 61.
- 81. Nowak. S, van der Mullen. J. J. A. M, van der Sijde. B, and Schram. D. C (1989), Spectroscopic determination of electron density and temperature profiles in an inductively coupled argon plasma, J. Quant. Spectroscop. Radiat. Transfer, 41, 177-192.
- 82. Fujimoto. T (1979), Kinetics of ionization-recombination of a plasma and population density of excited ions II. Equilibrium plasma, J. Phys. Soc. Jpn, 47, 273-281.
- 83. Parisi, A. F., Rayson, G. D., and Hieftje, G. M (1987), *Temporally and Spatially Resolved Studies in an Amplitude Modulated Inductively Coupled Plasma*. Spectrochim. Acta **42B**, 361-376.
- Marshall, K. A. and Hieftje, G. M (1987)., Measurement of True Gas-Kinetic
 Temperatures in an Inductively Coupled Plasma by Laser-Light Scattering.
 J. Anal. At. Spectrom., 2, 567-571,
- 85. Marshall, K. A and Hieftje,G. M(1988), Thomson Scattering for Determining Electron Concentrations and Temperatures in an ICP- II. Description and Evaluation of a Multichannel Instrument. Spectrochim. Acta **43B**, 851-865.

- 86. Mitchner, M and Kruger, C. H (1973), in "Partially Ionized Gases", Wiley, New York, p 67.
- 87. Thorne, A. P (1988), Spectrophysics. Chapman and Hall, London, p14.
- 88. George, C, Chan, C-Y, Gamez, G, Buscher, W and Hieftje, G. M (2008),

 Plasma diagnostic on a low-flow plasma for inductively coupled optical

 emission spectrometry, Spectrochim. Acta 63B (6), 619-629.
- 89. Griem, H. R (1964), Plasma Spetroscopy. McGraw-Hill, New York, p 91.
- 90. Nojiri, Y, Tanabe, K, Uchida, H, Haraguchi, H, Fuwa, K and Winefordner, J. D (1983), Comparison of spatial distributions of argon species number densities with calcium atom and ion in an inductively coupled argon plasma, Spectrochim. Acta 38B (1-2), 61-74.
- 91. Monning, C, A, Gebhart, B. D., Marshall, K. A., and Hieftje, G. M (1990).

 *Tomographic Image Reconstruction Techniques for Spectroscopic Sources: 2. Instrumentation. Spectrochim. Acta 45B(3), 261-270.
- 92. Parisi, A. F, Rayson, G. D, and Hieftje, G. M (1987), *Temporally and Spatially Resolved Studies in an Amplitude Modulated Inductively Coupled Plasma*. Spectrochim. Acta **42B**, 361-376.

- 93. de Olivares, D. R and Hieftje, G. M (1978), Saturation of Energy Levels in Analytical Atomic Fluorescence Spectrometry I. Theory. Spectrochim. Acta 33B, 79-99.
- 94. de Olivares, D.R. and Hieftje, G.M (1981), Saturation of Energy Levels in Analytical Atomic Fluorescence Spectrometry II. Experimental. Spectrochim. Acta **36B**, 1059-1079.
- 95. Hieftje, G. M, Rayson, G. D, and Olesik (1985), J. W, *A Steady-State Approach to Excitation Mechanisms in the ICP.* Spectrochim. Acta **40B**, 167-176.
- 96. Sheffield. J (1975), *Plasma scattering of Electromagnetic Radiation*, Academic Press, New York, p. 678.
- 97. Forster, H, Walter, J. N and Hume, D. N (1959), *Mutual Cation Interference Effects in Flame Photometry*: Anal. Chem. (31), 12, 2033-2036.
- 98. Zadgorska, Z and Krasnobaeva, N (1977), Influence of the anionic component of the additive on the relative intensity of atomic spectral lines in the analysis of dry residues from solutions, Spectrochim. Acta. 32B, 357-363.

- Kos'cielniak, P and Parczewski, A (1982), Theoretical model of alkali metals interferences in flame emission spectrometry, Spectrochim. Acta 37B, 881-887.
- 100. Zaranyika, M. F, Nyakonda, C, Moses, P (1991). Effect of excess sodium on the excitation of potassium in air-acetylene flame: a steady-state kinetic model which takes into account collisional excitation. Fresenius J. Anal. Chem, 341, 577-585.
- 101. Zaranyika, M. F. and Makuhunga, P (1997), A Possible Steady State Kinetic Model for the Atomization Process during Flame Atomic Spectrometry: Application to Mutual Atomization Interference Effects between Group I Elements. Fresenius J. Anal. Chem, 357, 249-257.
- 102. Zaranyika, M. F and Chirenje, A. T (1999), A possible steady-state kinetic model for the atomization process during flame atomic spectrometry:

 Application to atomization interference effects of alumimiun on Group II elements. Fresenius J. Anal. Chem, 364, 208-214.
- 103. Herrmann, R and Alkemade, C. T. J (1963), *Chemical Analysis by Flame Photometry*, Wiley-Interscience, New York, p 1
- 104. Boumans, P. W. J. M (1982), Comment on a proposed excitation mechanism in argon ICPs. Spectrochim Acta 37B, 75–82.

- 105. Blades, M. W, Coughlin, B. I, Walker, Z. H, Burton, J. J (1987), Excitation, Ionization and Spectral line Emission in the Inductively Coupled Plasma, prog. Analyt. Spectrosc. (10), 57-109.
- 106. Mills, J.W. and Hieftje, G.M (1984), A Detailed Consideration of Resonance Radiation Trapping in the Argon Inductively Coupled Plasma. Spectrochim. Acta 39B, 859-866.
- 107. Mermet J. M (1975), Excitation mechanisms of elements induced into a HF (high frequency) argon plasma, C. R. Acad. Sci., 281, 273-275.
- 108. Fujimoto. T (1979), Kinetics of Ionization-Recombination of a Plasma and Population Density of Excited Ions. I, Equilibrium Plasma, J. Phys. Soc. Japan, 47, 265-272.
- 109. Goldfarb. V. M (1981), *Developments in Atomic Plasma Spectrochemical Analysis*, Ed. R. M. Barnes, Heyden, London, p. 725.
- Eckert. H. U (1981), Developments in Atomic Plasma Spectrochemical Analysis, Ed. R. M. Barnes, Heyden, London, p. 35.
- Kirkbright. G. F (1981), Developments in Atomic Plasma Spectrochemical Analysis, Ed. R. M. Barnes, Heyden, London, p. 223.

- Boumans P. W. J. M (1982), Recent Advances in Analytical Spectroscopy,
 Ed. K. Fuwa, Pergamon Press, Oxford, p. 61.
- 113. Schram D. C, Raaymakers. I. J. M. M, van der Sijde. B, Schenkelaars. H. K. W and Bouman. P. W. J. M (1983), Approaches for clarifying excitation mechanisms in spectrochemical sources, Spectrochim. Acta 38B, 1545-1557.
- 114. de Galan L (1984), Some considerations on the excitation mechanism in the inductively coupled argon plasma, Spectrochim Acta 39B (4), 537-550.
- 115. Houk. R. S and Olivares. J. A (1984), General calculations of vertically-resolved emission profiles for analyte elements in inductively coupled plasmas, . Spectrochim. Acta 39 (4), 575-587.
- 116. Eljoundi. A, Batal. A and Mermet. J. M (1985), Dielectronic recombination in the zinc spectrum observed in inductively coupled plasma atomic emission spectroscopy, Spectrochim. Acta 40 (8), 1007-1011.
- 117. Hasegawa, T, and Haraguchi, H (1985), Collisional Radiative Model including radiation trapping and transport phenomena for diagnostics of an inductively coupled plasma, Spectrochim. Acta 40B, 1505-1515.

- 118. Blades M. W., Caughlin B. L., Walker Z. H. and Burton L. L (1987),
 Excitation, Ionization and Spectral Line Emission in the Inductively Coupled
 Plasma. Prog. Analyt Spectrosc, 10, 57-109.
- 119. Blades M. W., Caughlin B. L., Walker Z. H. and Burton L. L (1987), Excitation, Ionization and Spectral Line Emission in the Inductively Coupled Plasma, Prog. Analyt Spectrosc, 10, 57-109.
- 120. Blades, M.W (1987), *Inductively Coupled Plasma Emission Spectrometry.*Part III, Boumanns, P.W.J.M (ed.), Wiley Interscience, NY, p 387.
- 121. Olivares J. A. and Houk R. S (1986), Suppression of analytical signal by various concomitant salts in Inductively Coupled Plasma Mass Spectrometry. Anal. Chem, 58, 20-27.
- 122. Mermet J. M (1975), Excitation mechanism of elements induced into a HF (high frequence) argon plasma, C.R. Acad. Sci. B, 281, 273-275.
- Schram, D. C, Raaymakers, I. J. M. M, van der Sijde, B, Schenkelaars, H.
 K. W and Bouman P. W. J. M (1983). Approaches for clarifying excitation mechanisms in spectrochemical sources. Spectrochim. Acta 38B, 1545-1557.
- 124. Boumans, P. W. J. M (1969), *Theory of Spectrochemical Excitation*, Plenum Press, New York, p1.

- Rezaaiyaan, R, Olesik J. W, Hieftje G. M (1985). *Interferences in a Low-Flow, Low-Power Inductively Coupled Plasma*. Spectrochim. Acta 40B, 73-83.
- 126. Zaranyika, M. F and Chirenje, A. T (2000), A possible Steady-state kinetic model for the atomization and excitation processes during inductively coupled plasma atomic emission spectrometry: Application to interference effects of lithium on calcium, Fresenius J. Anal. Chem., 368, 45-51.
- 127. Wu, M. and Hieftje, G.M (1994), The Effect of Easily Ionized Elements on Analyte Emission Efficiency in Inductively Coupled Plasma Spectrometry.

 Spectrochim. Acta 49B(2), 149-161.
- 128. Chan,C-Y. and Hieftje, G. M (2004), Using Matrix Effects as a Probe for the Study of the Charge-Transfer Mechanism in Inductively Coupled Plasma-Atomic Emission Spectrometry. Spectrochim. Acta **59**(2), 163-183.
- 129. Chan, C-Y. and Hieftje, G. M (2008), *In-situ Determination of Cross-over*Point for Overcoming Plasma-related Matrix Effects in Inductively Coupled

 Plasma Atomic Emission Spectrometry. Spectrochim. Acta 63B, 355-356.
- 130. Chan, C-Y and Hieftje, G. M (2008), Use of Vertically Resolved Plasma

 Emission as an Indicator for Flagging Matrix Effects and System Drift in

 Inductively Coupled Plasma—Atomic Emission Spectrometry. J. Anal. At.

 Spec., 23 (2), 193-240.

- 131. Chan, C-Y and Hieftje, G. M (2008), Warning Indicators for the Presence of Plasma-related Matrix Effects in Inductively Coupled Plasma- Atomic Emission Spectrometry. J. Anal. At. Spec., 23 (2), 181-192.
- 132. Krzysztof. J and Malgorzata. D (2000), Study of an effect of easily ionizable elements on the excitation of 35 elements in Ar-MIP system coupled with solution nebulization, J. Anal. At. Spectrom, **15**, 269-276.
- 133. Chan, C-Y and Hieftje, G.M. (2006), Investigation of Plasma-Related Matrix

 Effects in Inductively Coupled Plasma-Atomic Emission Spectrometry

 Caused by Matrices with Low Second Ionization Potentials Identification of the Secondary Factor. Spectrochim. Acta 61B(6), 642-659.
- 134. Brockaert JAC, Leis F, Laqua K (1979). Some aspects caused by sodium tetraborate in the analysis of rare earth minerals with the aid of inductivley coupled plasma atomic emission spectrometry. Spectrochim Acta 34B, 167-175.
- 135. Hawatson, M (1976), *Introduction to Gas Discharge*₃2nd *Ed.* Pergamon Press, Oxford, p 55.
- 136. McDaniel, E. W (1964), *Collision phenomena in ionized gases*, Wiley and Sons, New York. P 1.

- 137. Hasegawa, T, Smith, B and Winefordner, J. D (1987), Quenching of Na resonance radiation; collisions of excited sodium with atoms, molecules and electrons in the ICP, Spectrochim. Acta: Atomic Spectroscopy 42B(10), 1093-1104.
- 138. Hasegawa, T and Haraguchi, H (1985), Appreciation of a collisional-radiative model for the description of an inductively coupled argon plasma, Spectrochim. Acta 40B(8), 1067-1084.
- 139. Rohatgi-Mukherjee KK (1978), *Fundamentals of Photochemistry*. Wiley, New York, p 7.
- 140. van der Mullen, J. A. M, Raaijmakers, I. K. M. M, van Lammeren, A. C. A. P, Schram, D. C, van der Sidje, B and Schenkelaars, H. J. W (1987), On the charge transfer in an inductively coupled plasma, Spectrochim. Acta. 42B(9), 1039-1051.
- 141. Burton, L. L and Blades, M. W (1991), Charge transfer between Ar and Mg in an inductively coupled plasma, Spectrochim. Acta 40B(6-7), 819-830.
- 142. Farnsworth, P. B, Smith, B. W, Omenetto, N (1991), An investigation of the balance of charge exchange between Mg and Ar ions in the ICP, Spectrochim. Acta 46B(6-7), 843-850.

- 143. Farnsworth, P. B, Woolley, A, Omenetto, N and Matveev, O (1999), Experimental studies of charge transfer reactions between argon and the third row metals calcium through copper in the inductively coupled plasma, Spectrochim. Acta 54B(14), 2143-2155.
- 144. Patricia, G, B and Carnahan, J. W (1994), *Charge transfer in analytical plasmas*, Spectrochim. Acta 49B(1), 105-115.
- 145. George, C, Chan C-Y, Hieftje, G. M (2004), Experimental evidence of stateselective charge transfer in inductively coupled plasma-atomic emission spectrometry, Spectrochim. Acta 59B(7), 1007-1020.
- 146. George, C, Chan, C-Y, Hieftje, G. M (2007), Investigation of charge transfer with non-argon gaseous species in mixed gas inductively coupled plasma-atomic spectrometry, Spectrochim. Acta 62B(3), 196-210.
- 147. Lovett, R. J (1982), *A rate model of Inductively coupled plasma analyte spectra*. Spectrochim. Acta 37B, 1969-1985.
- 148. Goldwasser, A and Mermert, J. M (1986), Contribution of charge transfer process to the excitation mechanisms in inductively coupled plasma atomic emission spectroscopy. Spectrochim Acta 41B, 725-739.
- 149. Allen CW (1955), Astrophysical Quantities, Athrone Press, London, p 1.

- 150. George, C, Chan, C-Y and Chan, W-T (2003), *Plasma-related matrix effects* in inductively coupled plasma-atomic emission spectrometry by group I and group II matrix-elements, Spectrochim. Acta 58B(7), 1301-1317.
- 151. Spectroflame Modula 90/95. Systems Operating Manual, Issue (90/95), Spectro Analytical Instruments, GmbH, Germany.
- 152. Winefordner, J. D, Schulman SG, O'Haver TC (1972), *Luminescence Spectrometry in Analytical Chemistry*, Wiley-Interscience, NY, p44.